A Model of Wind- and Buoyancy-Driven Ocean Circulation

ROLAND A. DE SZOEKE

Oregon State University, Corvallis, Oregon

(Manuscript received 7 September 1993, in final form 25 August 1994)

ABSTRACT

A layered model of steady geostrophic ocean circulation driven by wind stress and buoyancy flux at the surface is derived. Potential vorticity, or thickness, of the two near-surface layers is driven by Ekman pumping and buoyancy pumping. The latter is represented as a flow of mass proportional to the modified buoyancy flux, across the first submerged layer interface. This mass flux is modified by the advection of buoyancy in the wind-driven Ekman layer. Though diffusive diapycnal buoyancy flux across deeper layers is neglected at lowest order, it is essential for the global balance of the buoyancy budget. The global buoyancy balance requirement determines such parameters as the midocean outcrop latitudes of layers that outcrop in the subtropical gyre, and the depths of interfaces at the eastern boundary of layers that do not. These parameters control the mean thicknesses of the layers and, with the diapycnal diffusivity, the mean diffusive flux of buoyancy through each active layer. In this way the area-mean stratification is determined by the wind-driven circulation and the surface buoyancy flux.

Model solutions were computed for two idealized runs differing only by the amplitude of buoyancy forcing. In run A, the surface buoyancy flux was chosen to give a meridional buoyancy transport equivalent to 0.15 PW (1 PW = 1 petawatt) across the subtropical–subarctic gyre boundary. In run B, the buoyancy forcing was adjusted to give an intergyre meridional buoyancy transport equivalent to 0.51 PW. In both runs diapycnal diffusivities in the layers were held at $O(10^{-4}\ m^2\ s^{-1})$. These two runs gave density contrasts over the active layers of 8 kg m^{-3} (run A) and 18 kg m^{-3} (run B). The latter is an extremely large figure compared to the maximum density contrast across the ocean pycnocline observed in nature. The author concludes that the ocean cannot accomplish meridional buoyancy transports equivalent to O(1 PW), while diapycnal diffusivities are $O(10^{-4}\ m^2\ s^{-1})$ and density gradients across the pycnocline are $\leqslant O(4\ kg\ m^{-3}/1000\ m)$. It is necessary for global buoyancy and heat balance that there are regions in the oceans with far larger diapycnal diffusivities than $O(10^{-4}\ m^2\ s^{-1})$. Likely candidates for such regions are the upper layers of the ocean, where extremely powerful mixing can be driven by surface wind stirring and convection, and the high-energy zones of the western boundary currents.

1. Introduction

The qualitative manner in which wind stress drives ocean circulation on the rotating earth has been understood for forty years. That this circulation is confined within the main pycnocline (roughly, the upper kilometer) can be easily seen by inspecting transoceanic sections of density. The thickness of the pycnocline is controlled by the necessity of the ocean to maintain its heat, salt, and buoyancy budgets in balance. Many simple models assume a basic stratification of the ocean and impose on it wind-driven distortions to represent the circulation. Numerical models often embrace the full range of dynamical mechanisms that are thought important to the ocean circulation: wind stress, buoyancy forcing, turbulent diffusion, etc. For practical reasons, these models are usually started from states very close to the observed stratification of the natural ocean, or driven by Newtonian heating and salting boundary conditions that force them close to the observed distributions of surface temperature and salinity. This procedure begs the question of why the basic ocean stratification is the way it appears?

In this paper, the task is taken up of formulating a simple, steady, quasi-analytical, physical model of ocean circulation that contains the minimal dynamical features necessary to represent and explain the stratification and circulation in terms of wind stress and surface-buoyancy forcing. The ocean stratification is represented by a set of discrete density layers, some of which outcrop at the surface. The surface layer is forced by the wind stress curl and the surface buoyancy flux. The latter is equivalent to conversion, at a rate proportional to the modified surface buoyancy flux, of water from the subsurface density layer into water of the surface density layer, or vice versa if surface buoyancy flux is upward (Veronis 1978; Luyten and Stommel 1986). The model dynamics explicitly take account only of geostrophic motions, so the surface buoyancy flux must be modified by the divergence of horizontal

Corresponding author address: Dr. Roland A. de Szoeke, College of Oceanic and Atmospheric Sciences, Oregon State University, Oceanography Admin. Bldg. 104, Corvallis, OR 97331-5503.

buoyancy transport in the Ekman layer. If buoyancy crosses the sea surface, then that buoyancy must cross submerged isopycnal surfaces (layer interfaces) for the intervening layers not to be lightened. This diapycnal buoyancy flux is accomplished in the model by specifying a conventional parameterization of diffusivity multiplied by buoyancy gradient, expressed in appropriate layer-discretized form. However, by neglecting diapycnal fluxes at lowest order (except the surface flux), we obtain a system much like the ventilated circulation models of Luyten et al. (1983, hereafter LPS), Talley (1985), and de Szoeke (1987, 1992), in which potential vorticity is approximately conserved in submerged layers. After obtaining the lowest-order circulation, we use the integral constraint on each layer that the net throughput of buoyancy must be in balance (impossible without the reinstatement of diapycnal buoyancy fluxes) to determine such parameters as the meridional outcrop spacings (for layers that outcrop in the subtropics), or layer thicknesses along the eastern boundary (for layers outcropping in the subarctic). These parameters, arbitrarily chosen by LPS, Talley (1985), and de Szoeke (1992), control the mean thicknesses of the layers and, hence, the discretized mean density gradient of the ocean. We find these parameters by a trial and error method in which we continually refine choices and recalculate the mass and buoyancy circulations until buoyancy balance is achieved.

The theory of the circulation model is derived in the following sections. Particularly novel is the inclusion of surface buoyancy forcing and diapycnal buoyancy flux, and the use of these, with the constraint of area-integrated buoyancy balance, to determine the mean stratification. We applied the model to an idealized double-gyre circulation system. Two runs will be discussed: one in which the buoyancy forcing is quite modest (equivalent to 0.15 PW subtropic to subarctic heat transport, if buoyancy were due solely to temperature), and one in which buoyancy forcing is fairly strong (equivalent to 0.51 PW subtropic–subarctic heat transport). In both runs we insisted on diapycnal diffusivities no larger than $O(10^{-4}\ m^2\ s^{-1})$. This led to a fairly strong density stratification in the first case and an extremely strong stratification (many times stronger than observed in nature) in the second. There is a simple nexus between buoyancy (or heat) throughput on one hand, and diffusivity and density stratification on the other. To achieve realistic density stratification for buoyancy throughput equivalent to O(1 PW) requires diffusivities far larger than can be justified from measurements of turbulent microstructure in the ocean (Gregg 1987). The main practical result of this paper is to pose the following dilemma. If the oceans really process meridional buoyancy transports equivalent to O(1 PW) heat transport, as compilations of climatological air–sea fluxes (Esbensen and Kushnir 1981; Isemer and Hasse 1987) and direct estimates of oceanic heat transport (Bryan 1962; Bennett 1978; Bryden and Hall 1980; Bryden et al. 1991; Toole and Warren 1993) suggest, where can the necessary diapycnal diffusivities in the ocean much larger than $O(1 \times 10^{-4}\ m^2\ s^{-1})$ be found? Leading candidates are the upper layers of the ocean where very strong episodic mixing can be generated by surface wind stirring and convection (de Szoeke 1980), and the western boundary currents where strong shears may generate energetic turbulence.

2. The model

Let us represent the ocean by a stack of layers labeled $m, m+1, \ldots, j, \ldots, n, n+1$, with densities $\rho_m, \ldots, \rho_j, \ldots, \rho_n, \rho_{n+1}$ (Fig. 1). The base of the jth layer intersects the surface ("outcrops") along the line $y = Y_j(x)$. The depth of the base of the jth layer, the interface between densities ρ_j, ρ_{j+1}, is $z = -H_j(x, y)$.

In the limit of infinitely closely spaced densities, the interfaces would correspond to isopycnal surfaces. Following Gent and McWilliams (1990) and de Szoeke and Bennett (1993), we take these to be surfaces of equal density averaged over the scales of microstructure turbulence (nominally, spatial scales smaller than 10 m with a horizontal to vertical aspect ratio close to unity and timescales shorter than the buoyancy pe-

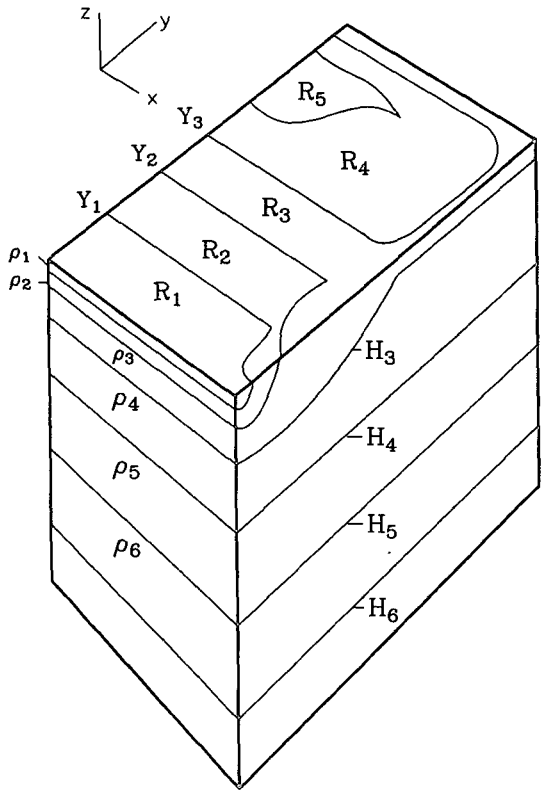

FIG. 1. Schematic of the wind- and buoyancy-driven pycnocline model in an ocean with a subtropical–subarctic gyre pair.

riod). The unresolved microstructure scales can affect diapycnal exchange of material. Further averaging, over mesoscale eddy variability, is taken with respect to these fluctuating isopycnals, not with respect to fixed levels. From this frame of reference, mesoscale variability does not contribute to average diapycnal material exchange. In the momentum balance, velocity fluctuation correlations on isopycnals produce additional eddy momentum transport divergence terms similar in form to the conventional Reynolds stress terms. We shall neglect these terms except in an implicit surface Ekman boundary layer. In what follows, the horizontal layer velocities that appear are the thickness-weighted mesoscale-average velocities $\hat{\mathbf{u}}_j = \overline{h_j \mathbf{u}_j}/\bar{h}_j$ (though we shall drop the caret, and the bars on the mean thickness $\bar{h}_j = \bar{H}_j - \bar{H}_{j-1}$ and mean pressure $\bar{p}_j$). The averages are carried out within a fluctuating isopycnal layer. Thickness-weighted averaging produces novel pressure gradient/thickness correlation terms $-\overline{h_j' \nabla p_j'}/\rho_0 \bar{h}_j$ in the mesoscale-average momentum balance in isopycnal layers (de Szoeke and Bennett 1993). These are probably negligible except in regions of high mesoscale eddy variability, like boundary currents, which our model does not cover, and are omitted in the geostrophic balance, which we shall assume. This careful, precise specification of mesoscale-average isopycnals is crucial to our identification of the diapycnal flows in the model solely with diffusive microstructure processes and not with mesoscale eddy processes.

As stated, motion is taken to be geostrophic and hydrostatic in each layer:

$$-fv_j = -p_{jx}/\rho_0, \quad fu_j = -p_{jy}/\rho_0, \quad p_{jz} = -g\rho_j. \tag{2.1a,b,c}$$

It is convenient to restrict the discussion for the moment to the subtropical gyre, in which all the layers with indices in the range $m \leqslant j \leqslant n-1$ are assumed to appear at the surface. The $(n+1)$th layer, we shall suppose, is motionless. By integrating the hydrostatic relation from this motionless layer, in which the horizontal pressure gradient is zero, we can see that the pressure in each layer is, within a constant,

$$p_j = -\rho_j g z + \rho_0 P_j(x, y) \tag{2.2}$$

for $m \leqslant j \leqslant n$, where, with $\gamma_j = g(\rho_{j+1} - \rho_j)/\rho_0$,

$$P_j = \gamma_n H_n + \gamma_{n-1} H_{n-1} + \cdots + \gamma_j H_j \tag{2.3}$$

is the Montgomery potential for each layer. Hence Eqs. (2.1a,b) become

$$-fv_j = -P_{jx}, \quad fu_j = -P_{jy}. \tag{2.4a,b}$$

The conservation of mass in the jth layer, allowing for cross-isopycnal flows e_j, e_{j-1} across the jth and $(j-1)$th interfaces, is governed by

$$\nabla \cdot (\mathbf{u}_j h_j) = e_j - e_{j-1}, \tag{2.5}$$

where $h_j = H_j - H_{j-1}$. This is a discrete version of the steady thickness equation derived by de Szoeke and Bennett (1993). Substituting (2.4), we can write this as

$$J\left(P_j, \frac{h_j}{f}\right) = e_j - e_{j-1}, \tag{2.6}$$

which is a form of the potential vorticity balance equation. We shall call h_j/f the potential thickness of the jth layer. Denote by R_k the region where layer k occurs at the surface, $Y_{k-1}(x) \leqslant y \leqslant Y_k(x)$. Then in R_k we identify the flow across the ocean surface:

$$e_{k-1} = \hat{\mathbf{z}} \cdot \nabla \times (\boldsymbol{\tau}/\rho_0 f) \equiv w_{\mathrm{Ek}}, \tag{2.7a}$$

with the Ekman pumping velocity. Otherwise, the e_j are related to the divergences of buoyancy fluxes due to microstructure turbulence. The latter can be written using discrete analogues of de Szoeke and Bennett's (1993) forms for the diapycnal microstructure buoyancy fluxes $F_j = (g/\rho_0)(\overline{e_* \rho_*})_j$ in each layer. (Starred subscripts denote fluctuations due to microstructure.) In terms of diapycnal diffusivity coefficients K_j, this gives

$$\gamma_k e_k = B_0' - F_{k+1}, \quad j = k \tag{2.7b}$$

$$\gamma_j e_j = F_j - F_{j+1}, \quad j > k, \tag{2.7c}$$

where

$$F_j = \frac{g}{\rho_0} K_j(\rho_{j+1} - \rho_{j-1})/2h_j, \quad j > k. \tag{2.7d}$$

The buoyancy flux across the surface layer $F_k = B_0'$ is an exception to (2.7d); it must be the air–sea buoyancy flux at the ocean surface, but modified by the divergence of buoyancy transport, within the surface layer, by Ekman currents, which are not part of the geostrophic currents countenanced by (2.1) (Nurser and Marshall 1991). The necessary modifications are shown for discrete layers in appendix A. It is convenient to call B_0' the buoyancy pumping. For $j \geqslant n$, the diapycnal velocities e_j are taken to be zero. This is equivalent to assuming that the eddy diffusivities K_j are zero for $j \geqslant n$. Yin et al. (1992) considered a layered model represented by equations similar to the above.

By summing the potential vorticity balances (2.6) over all moving layers from the nth to the kth, we obtain the Sverdrup transport relation in the form

$$\frac{\beta}{2f^2} \partial_x(\gamma_n H_n^2 + \gamma_{n-1} H_{n-1}^2 + \cdots + \gamma_k H_k^2) = w_{\mathrm{Ek}}. \tag{2.8}$$

This can be integrated to give

$$\Theta_k \equiv \gamma_n H_n^2 + \gamma_{n-1} H_{n-1}^2 + \cdots + \gamma_k H_k^2 = \Theta(x, y) + \Phi(y), \tag{2.9}$$

where

$$\Theta(x, y) = -\int_x^a \frac{2f^2}{\beta} w_{Ek}(x', y)dx' \quad (2.10)$$

and

$$\Phi(y) = \int_y^b \frac{-2\tau^y(a, y')}{\rho_0} dy' + \{\gamma_n H_n^2 + \cdots + \gamma_k H_k^2\}_{\substack{y=b \\ x=a}}. \quad (2.11)$$

The latter contribution, $\Phi(y)$, ensures that the onshore geostrophic transport at the eastern boundary, $x = a$, namely,

$$\frac{1}{2f}\frac{\partial \Theta_k}{\partial y} = \frac{1}{f}\left(h_n \frac{\partial P_n}{\partial y} + \cdots + h_k \frac{\partial P_k}{\partial y}\right) = h_n u_n + \cdots + h_k u_k, \quad (2.12)$$

balances the offshore Ekman transport $\tau^y(a, y)/f\rho_0$ (de Szoeke 1992).

Suppose we neglect the diffusivity-driven cross-isopycnal fluxes, that is, formally set the diffusivity coefficients K_j in (2.7) to zero. Then, except for $j = k$, $k + 1$, the right side of (2.6) is zero, and we can write

$$\frac{h_j}{f} = \Gamma_j(P_j), \quad j > k + 1, \quad (2.13)$$

where the functions Γ_j remain to be determined. Lines of constant h_j/f and P_j are called the geostrophic contours of layer j. We can manipulate Eq. (2.6) for $j = k + 1$,

$$J\left(P_{k+1}, \frac{h_{k+1}}{f}\right) = -e_k, \quad (2.14)$$

into a more convenient form by making use of (2.8) and (2.13). By repeated use of (2.13) and (2.3), we can write H_k, P_k as functions of H_n and f for $k + 1 \leqslant j \leqslant n - 1$:

$$\left.\begin{aligned} H_{n-1} &= H_n - f\Gamma_n(P_n) = H_{n-1}(H_n, f) \\ H_{n-2} &= H_{n-1} - f\Gamma_{n-1}(P_{n-1}) = H_{n-2}(H_n, f) \\ &\vdots \\ H_{k+1} &= H_{k+2} - f\Gamma_{k+2}(P_{k+2}) = H_{k+1}(H_n, f). \end{aligned}\right\} \quad (2.15)$$

These equations, with (2.3), represent an implicit solution for the discretely layered form of the equations in continuous density coordinates:

$$-\frac{1}{f}\frac{\partial z}{\partial \rho} = \Gamma(P, \rho), \quad \frac{\partial P}{\partial \rho} = gz,$$

with boundary condition $P(\rho_{n+1}) = 0$ (Huang 1988).

In what follows, it will be useful to introduce notation for partial derivatives with respect to H_n and f:

$$H_j' = \frac{\partial}{\partial H_n} H_j(H_n, f), \quad \hat{H}_j = \frac{\partial}{\partial f} H_j(H_n, f); \quad (2.16)$$

similarly for derivatives of the P_j. We shall use (2.15) to rewrite the terms on the left side of (2.14):

$$J\left(P_{k+1}, \frac{H_{k+1}}{f}\right) = \left\{\frac{1}{f}(P_{k+1}'\hat{H}_{k+1} - \hat{P}_{k+1}H_{k+1}') - \frac{1}{f^2}P_{k+1}'H_{k+1}\right\}\beta H_{nx}, \quad (2.17)$$

$$-J\left(P_{k+1}, \frac{H_k}{f}\right) = -\frac{1}{f}J(P_{k+1}, H_k) + \frac{\beta}{f^2}P_{k+1}'H_kH_{nx} = -\frac{1}{f}P_{k+1}'(H_{nx}H_{ky} - H_{ny}H_{kx}) + \frac{\beta}{f}\hat{P}_{k+1}H_{kx} + \frac{\beta}{f^2}P_{k+1}'H_kH_{nx}. \quad (2.18)$$

We see that (2.17) and (2.18) involve the partial derivatives H_{kx}, H_{ky}, H_{nx}, H_{ny}. We shall use the Sverdrup relation (2.9) to relate ∇H_n to ∇H_k. Note that the partial sum

$$\Theta_{k+1} \equiv \gamma_n H_n^2 + \cdots + \gamma_{k+1}H_{k+1}^2 \quad (2.19)$$

is, because of (2.15), a function of H_n, f. Hence (2.9), rewritten as

$$\Theta_{k+1}(H_n, f) + \gamma_k H_k^2 = \Theta(x, y) + \Phi(y), \quad (2.20)$$

can be used to relate H_n and H_k. Taking the gradient of (2.20), we obtain

$$\Theta_{k+1}'\nabla H_n + \hat{\Theta}_{k+1}\beta\mathbf{j} + 2\gamma_k H_k \nabla H_k = \nabla(\Theta + \Phi). \quad (2.21)$$

We use this to eliminate H_{nx}, H_{ny} from (2.17) and (2.18). After a great deal of tedious manipulation, (2.14) can be put in the form

$$(\mathbf{U}_n + c_{k+1|n}\mathbf{i})\cdot\nabla H_k = a_{k+1|n}e_k + b_{k+1|n}e_{k-1}, \quad (2.22)$$

where

$$\mathbf{U}_n = \frac{1}{2fH_n}(-\partial_y, \partial_x)(\Theta + \Phi), \quad (2.23)$$

$$c_{k+1|n} = -\frac{\beta}{fH_n} \times \left[\left\{\frac{H_{k+1} - H_k}{f} - \frac{P_{k+1}'\hat{H}_{k+1} - \hat{P}_{k+1}H_{k+1}'}{P_{k+1}'}\right\}\gamma_k H_k - \frac{P_{k+1}'\hat{\Theta}_{k+1} - \hat{P}_{k+1}\Theta_{k+1}'}{2P_{k+1}'}\right], \quad (2.24)$$

$$a_{k+1|n} = \frac{1}{2H_n}\frac{\Theta_{k+1}}{P_{k+1}'}, \quad (2.25)$$

$$b_{k+1|n} = -\left\{\frac{H_{k+1} - H_k}{f} - \frac{P_{k+1}'\hat{H}_{k+1} - \hat{P}_{k+1}H_{k+1}'}{P_{k+1}'}\right\}\frac{f}{H_n}. \quad (2.26)$$

The coefficients c, a, b can, because of (2.15) and (2.20), be thought of as functions of H_k, as well as the geographic coordinates x, y. An observer moving with the velocity given by

$$\frac{d\mathbf{x}_{k+1}}{dt} = \mathbf{U}_n + c_{k+1|n}\mathbf{i} \tag{2.27}$$

which follows a characteristic trajectory along H_k appears to change by (2.22); that is,

$$\frac{dH_k}{dt} = a_{k+1|n}e_k + b_{k+1|n}e_{k-1}. \tag{2.28}$$

The interpretation of the observer's trajectory (2.27) is interesting. It is composed of two parts: the Sverdrup transport $\mathbf{U}_n$ averaged over the depth of the totality of moving layers H_n, and the generalized long Rossby wave propagation speed $c_{k+1|n}$. The latter has a familiar form for the case of two moving layers, $n = k + 1$. In that case $\hat{H}_n = \hat{P}_n = \hat{\Theta}_n = 0$, while $H'_n = 1$, $P'_n = 2\gamma_n$, $\Theta'_n = \gamma_n H_n$, so that $c_{n|n}$ becomes

$$c_{n|n} = -\frac{\beta\gamma_{n-1}}{f^2}\left\{\frac{1}{H_{n-1}} + \frac{1}{H_n - H_{n-1}}\right\}^{-1}. \tag{2.29}$$

This is the well-known two-layer long Rossby wave speed. In the same two-layer context,

$$a_{n|n} = 1 \quad \text{and} \quad b_{n|n} = -\frac{H_n - H_{n-1}}{H_n}. \tag{2.30}$$

For two layers, Eqs. (2.27), (2.28) thus reduce to Luyten and Stommel's (1986) circulation equations for wind and buoyancy forcing. On the other hand, in the general case for an arbitrary number of layers, Eqs. (2.27), (2.28), together with the Sverdrup relation (2.9), and the potential thickness relations (2.13), represent a complete system for the determination of all the layer interface depths H_j.

When $e_k = 0$ (no buoyancy forcing), it can be shown that h_{k+1}/f is conserved along the characteristics given by (2.27). Hence, the characteristics coincide with the geostrophic contours for layer $k + 1$ in this case. When $e_k \neq 0$, so that potential thickness in layer $k + 1$ is not conserved, the characteristics represent a generalization of the idea of geostrophic contours. For this reason we associate the characteristic $\mathbf{x}_{k+1}(t)$ with the index of the next-to-surface layer $k + 1$. Although the geostrophic contours of a deeper layer are also characteristics of the p.d.e. for that layer, we shall reserve the term for the next-to-surface layer. Does the surface layer possess characteristics? The question need not arise because the surface layer potential thickness equation has been replaced by the sum of equations over all layers. This gave the Sverdrup transport relation (2.8), whose characteristics are merely constant latitude lines.

a. Specification of potential thickness relations and layer outcrops

It remains to determine the functional relations $\Gamma_j(P_j)$ between the potential thicknesses and Montgomery pressures in (2.13). This is only an issue in the anticyclonic part of the circulation gyre where surface waters tend to be pushed equatorward and subducted under lighter water. So the functions are specified along outcrops like $Y_j(x)$, where $H_j = 0$, and where layer $j + 2$ water is about to pass beyond the direct influence of wind stress (surface layer) and buoyancy flux (surface and next-to-surface layers) and thence conserve its potential thickness. LPS were able to choose the $Y_j(x)$ to be constant latitudes. However, de Szoeke (1992) showed that under conditions where the alongshore wind at the eastern boundary is nonzero the proper satisfaction of the eastern boundary conditions determines the shapes of the outcrops $Y_j(x)$ near the boundary, given only their eastern boundary intersections y_j^e. This influence on $Y_j(x)$ [and $\Gamma_{j+2}(P_{j+2})$] extends only a finite distance into the ocean, beyond which the outcrops may be taken to be constant latitudes y_j^w. De Szoeke's (1992) treatment needs to be modified to take account of buoyancy forcing. This is done in appendix B.

b. Western boundary conditions

For a layer k that surfaces in the northern portion of the subtropical gyre, the condition

$$U_n + c_{k+1|n} > 0 \tag{2.31}$$

holds along the western boundary, $x = 0$. In this situation we must assign "initial" values for the surface and next-to-surface layer depths H_k, H_{k+1} at the western boundary. This is done as follows. The potential thickness of the submerged layer is chosen to be constant along the western boundary

$$(H_{k+1} - H_k)/f = \{H_{k+1}/f\}_{(0,Y_k(0))}. \tag{2.32}$$

This requirement, with the Sverdrup relation (2.9), serves to determine H_k, H_{k+1} along the portion of the western boundary where layer k is at the surface. (The deeper layers, $H_{k+2}, \ldots, H_n$, are determined by their potential thickness–pressure relations.) The region of layer $k + 1$ covered by characteristics that originate at the western boundary is called the western shadow zone. Condition (2.32) is motivated by LPS's requirement that such layers [satisfying (2.31)] have homogeneous potential thickness. In the case of nonzero buoyancy forcing, $e_k > 0$, Eq. (2.22) [or Eq. (2.14)] shows that the constant potential thickness value (2.32) enforced at the western boundary does not persist throughout the western shadow zone. As the characteristics of layer $k + 1$ in the western shadow zone pass under $y = Y_{k-1}(x)$, the potential thickness–pressure relation for that part of layer $k + 1$ is determined in the same way as described above.

As noted in appendix B, an exception to this rule applying a western boundary condition is made for the layer (labeled 4 in appendix B), which does not surface in the subtropics but is forced by buoyancy flux (and would be stagnant otherwise).

3. Circulation in the subarctic

We now turn to the theory of circulation in the subarctic. Because the meridional component of the Sverdrup flow is poleward, characteristic trajectories [Eq. (2.27)] move poleward. Because Ekman pumping is upward, surface layers tend to shoal along these characteristics. This effect is exacerbated by generally negative surface buoyancy flux, which also tends to diminish the surface layer thickness. Hence, the surface layer tends to shoal to nothing, to be replaced as surface layer by the next denser layer. This leads to a nesting of ever denser outcropping layers in the subarctic.

First, we shall define what we mean by the terms "subarctic" and "subtropical." Consider the region R_{n-1} in which layer $n-1$ is found at the surface and overlies layer n, the only other O(1) moving layer. In this region Ekman pumping reverses sign along some line (Fig. 2); that is, from (2.23),

$$H_n V_n = \beta^{-1} f w_{\mathrm{Ek}} = 0. \tag{3.1a}$$

Now U_n is usually positive in the vicinity of $w_{\mathrm{Ek}} = 0$, though decreasing towards the east, while $c_{n|n} < 0$, so that somewhere along this line

$$U_n + c_{n|n} = 0. \tag{3.1b}$$

[If this does not occur, then we look in the adjacent regions R_n *or* R_{n-2}. In other words, conditions are allowed to *define* the index n.] The conditions (3.1a,b) describe a point for the differential equation (2.22) at which four stagnant characteristics meet, two arriving (one each from the eastern and western boundaries), and two departing. Because $|\mathbf{U}_n + c_{n|n}\mathbf{i}| = 0$ at the stagnant point, an "observer" following any of the four characteristics takes forever to arrive or depart from it. All other layer-n characteristics are first attracted to, and then repelled by the stagnant point, called the "Rossby attractor." The regions north and south of the pair of stagnant characteristics approaching the Rossby attractor are called the subarctic and subtropics, respectively (Fig. 2). If the zero Ekman pumping line is zonal, that is, along $y = b$, then these stagnant characteristics will coincide with $y = b$. The circulation in the subarctic (subtropical) region will then be entirely cyclonic (anticyclonic). Otherwise, circulation in the subarctic (subtropical) region will be mostly cyclonic (anticyclonic), though with a small wedge between the stagnant characteristic and the zero Ekman pumping line where it is anticyclonic (cyclonic).

Now we integrate Eq. (2.22) [or (2.27), (2.28)] in the subarctic region for $k = n - 1$. Equations (2.29), (30) give $c_{n|n}$, $a_{n|n}$, $b_{n|n}$. Except in the small anticyclonic wedge, Ekman pumping is positive, $e_{n-2} = w_{\mathrm{Ek}} > 0$. If the buoyancy forcing is negative, then $e_{n-1} < 0$. Both terms on the right side of (2.28) are negative and tend to reduce the surface layer depth H_{n-1} along the characteristics given by (2.27). Eventually the surface layer depth may dwindle to zero. This will define an outcrop line for layer $n-1$; namely, $y = Y_{n-1}(x)$ [or $x = X_{n-1}(y)$ if the outcrop is multivalued as a function of x] and a boundary for region R_{n-1}. Beyond $Y_{n-1}(x)$, in region R_n, the surface and next-to-surface layers have indices n, $n+1$. The layer depths in this region are described by Eqs. (2.9), (2.22) with n replaced by $n+1$, and $k = n$. These equations can be integrated throughout R_n following layer $n+1$ characteristics given by Eq. (2.27), with n replaced by $n+1$ and $k = n$. Buoyancy forcing e_n puts layer $n+1$, inert in regions $R_{n-1}, R_{n-2}, \ldots$, into motion in R_n. Along $y = Y_{n-1}(x)$, the characteristics are initialized by the terminal values of H_n from the integration along layer n characteristics in R_{n-1}; H_{n+1} is given by $H_{n+1}(a, b)$, the constant value of the depth of layer $n+1$ throughout regions $R_{n-1} \ldots$, and in particular along the eastern boundary. The surface layer depth H_n in region R_n may also decline to zero along layer $n+1$ characteristics. This defines the subarctic outcrop $Y_n(x)$ of layer n. To integrate beyond $Y_n(x)$ into region R_{n+1} we simply repeat the procedure outlined. In this way we may get a nest of ever denser outcropping regions $R_{n-1}, R_n, R_{n+1}, \ldots, R_N$ in the subarctic. The index N refers to the densest outcropping layer in the subarctic. At any point in the subarctic only two layers are in motion, the surface and next-to-surface layers.

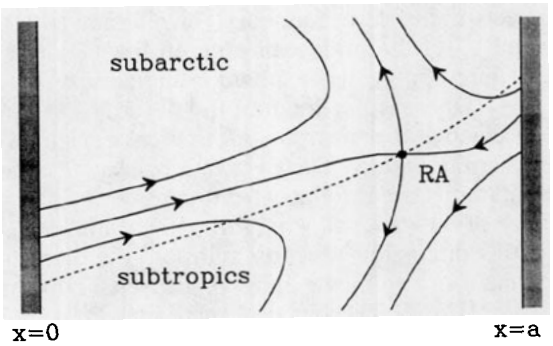

FIG. 2. The Rossby attractor (RA), where $\mathbf{U}_n + c_{n|n}\mathbf{i} = 0$, and the zero Ekman pumping line $w_{\mathrm{Ek}} = 0$ (dashed). Regions of positive and negative Ekman pumping are north and south of this line. The characteristics arriving at RA from the eastern and western boundaries define the boundary between subarctic and subtropical regions. Note that subarctic (subtropical) is not synonymous with positive (negative) Ekman pumping.

4. Balancing the global buoyancy budgets

There remains a number of arbitrary parameters, one associated with each layer. For each layer j that outcrops in the subtropical gyre, that is, for $j \leq n-2$, there is the arbitrary latitude y_j^e at which the outcrop

intersects the eastern boundary (or alternatively, the latitude y_j^w of the midocean outcrop line). For each layer j outcropping in the subarctic circulation, that is, $j \geq n-1$, there is the depth of that layer $H_{j0} \equiv H_j(a, b)$, specified at the subarctic–subtropical transition on the eastern boundary. There is a rational way to choose these parameters; it follows from considering the net balance of buoyancy flowing through each layer.

In this discussion we must reinstate the diapycnal velocities e_j driven by the diffusive diapycnal buoyancy fluxes F_j [Eq. (2.7)], but neglected after Eq. (2.13). Yin et al. (1992) studied a layered model of deep-water formation, similar in its basic form to the present one. However, they considered the contributions to the cross-isopycnal flows only of deviations of the dependence of fluxes F_j on layer depths h_j from some static background state; the effects of which were discarded.

a. Buoyancy balance

1) LAYER 1

We begin with the layer, arbitrarily labeled 1, which we take to be the lightest layer, abutting the equatorward boundary, at which there is no normal transport. Water crosses the base of layer 1 at rate e_1 per unit area and is exported (or imported) across the outcrop Y_1 by the Ekman transport at rate E_1 [Eq. (A3)]. For steady state these mass sources and sinks must balance

$$-E_1 + \int_{R_1} e_1 dA = 0 \tag{4.1}$$

(Fig. 3). Now e_1 is given by (2.7b) for $k = 1$:

$$e_1 = (B_0' - F_2)/\gamma_1, \quad \text{in} \quad R_1 : y < Y_1, \tag{4.2}$$

where B_0' is the modified surface flux and F_2 is given by (2.7d). The integral over R_1 of the modified buoyancy flux (A2) is, because of (A5),

$$\int_{R_1} B_0' dA = \int_{R_1} B_0 dA + \gamma_1 E_1. \tag{4.3}$$

Then (4.1)–(4.3) give

$$\int_{R_1} B_0 dA = \int_{R_1} F_2 dA. \tag{4.4}$$

This expresses the simple fact that, in steady state, the total buoyancy received at the sea surface by layer 1 must be balanced by the area-integrated diffusion of buoyancy F_2 through layer 2. The volume balance statement (4.1) is evidently equivalent to the buoyancy balance statement (4.4). Though e_1 is given in terms of the modified buoyancy flux B_0', it is the net surface buoyancy flux B_0 that appears in (4.4). The diversion of surface buoyancy flux to alter the Ekman transport across the outcrop Y_1, while important to the internal redistribution of layer 1, does not figure in its integrated buoyancy balance.

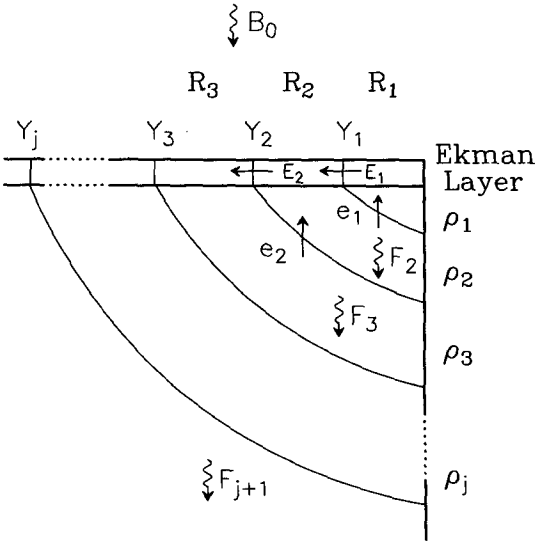

FIG. 3. Schematic illustrating that the surface buoyancy flux, integrated over waters lighter than a certain value, must be balanced by the diffusive flux integrated over the submerged interface separating the lighter waters from the denser waters. See Eq. (4.11).

2) LAYER 2

Next, we consider the mass budget of the next denser layer, labeled 2. This is given by

$$-E_2 + E_1 + \int_{R_2 \cup R_1} e_2 dA - \int_{R_1} e_1 dA = 0, \tag{4.5}$$

(Fig. 3) where E_2 is the Ekman transport across outcrop Y_2, and

$$e_2 = (B_0' - F_3)/\gamma_2, \quad \text{in} \quad R_2 : Y_1 < y < Y_2 \tag{4.6a}$$

$$= (F_2 - F_3)/\gamma_2, \quad \text{in} \quad R_1 : y < Y_1, \tag{4.6b}$$

with F_2, F_3 given by (2.7d). By adding (4.1) and (4.5), we obtain

$$-E_2 + \int_{R_2 \cup R_1} e_2 dA = 0. \tag{4.7}$$

Also, similar to (4.3), we obtain

$$\int_{R_2} B_0' dA = \int_{R_2} B_0 dA + \gamma_2 E_2. \tag{4.8}$$

Hence, (4.7) may be written

$$\int_{R_2} B_0 dA + \int_{R_1} F_2 dA = \int_{R_1 \cup R_2} F_3 dA, \tag{4.9}$$

or, by adding (4.4),

$$\int_{R_1 \cup R_2} B_0 dA = \int_{R_1 \cup R_2} F_3 dA. \tag{4.10}$$

3) LAYER j

Indeed, this argument may be repeated for any layer that outcrops, for example, layer j, to the effect that

$$\int_{\substack{\cup R_k \\ k\leqslant j}} B_0 dA = \int_{\substack{\cup R_k \\ k\leqslant j}} F_{j+1} dA, \qquad (4.11)$$

where F_{j+1} is given by (2.7d). Equation (4.11) illustrates a fundamental buoyancy balance principle of the stratified ocean. The buoyancy acquired through air–sea exchange at the ocean surface by all layers lighter than, and including, the jth must balance the diffusion of buoyancy through the $(j+1)$th layer. The fundamental importance of diapycnal diffusion to the maintenance of the buoyancy balance is clear. Without it, it would be impossible to accommodate a nonzero distribution of buoyancy flux into the ocean surface. The relation (4.11) may be readily generalized to the continuously stratified ocean (Speer and Tziperman 1992). The validity of (4.11) does not depend on the parameterization (2.7d) of diapycnal fluxes. Nor does it depend on the quite mild neglect of the divergence of along-isopycnal fluxes in (2.7b,c), because the area integral in (4.11) ensures their disappearance. For example, the parameterization of alongisopycnal buoyancy flux, which Gent and McWilliams (1990) proposed, would have no effect on the appearance of (4.11). Still, the parameterization (2.7d) relating buoyancy fluxes to density gradients by means of diapycnal diffusivity coefficients provides a convenient closure of the problem, one that has considerable empirical basis in oceanic microstructure measurements (Gregg 1987; Ledwell et al. 1993). We emphasize that with the definition of average isopycnal surfaces (or discrete layer interfaces) given in section 2, only microstructure processes can contribute to the diapycnal buoyancy flux in (4.11).

A special case of (4.11) is for $j = N$, the densest layer to outcrop at the ocean surface in the subarctic. Then the left side of (4.11) is the integral of buoyancy flux over the entire area of the ocean. For steady state, this must vanish. Indeed, we shall require surface buoyancy flux fields to satisfy

$$\int_{\substack{\cup R_k \\ k\leqslant N}} B_0 dA = 0. \qquad (4.12)$$

This requires that the right side of (4.11) also vanish for $j = N$. We effect this in our model by setting $K_{N+1} = 0$ in (2.7d), that is, no diffusion in layers below the densest outcropping layer.

b. *Determining the stratification*

The imposition of the buoyancy balance requirement (4.11) for each layer settles the last remaining indeterminacies in the model. These were the midocean outcrop latitudes y_j^w of layers that outcrop in the subtropics (or, equivalently, the eastern boundary intersections y_j^e of the outcrops) and the choice at the eastern end of the subtropic–subarctic boundary of the depths of deeper layer interfaces H_{j0} that do not outcrop in the subtropics. The qualitative way in which these parameters influence (4.11) can be easily seen. By increasing $H_{j+1,0}$ or y_{j+1}^w, whichever parameter is appropriate, the average thickness of layer $j+1$ tends to be increased (Fig. 3). This reduces the right side of (4.11). Conversely, by decreasing $H_{j+1,0}$ or y_{j+1}^w the right side of (4.11) can be enhanced. So by varying these parameters, the balance (4.11) can be achieved. (Of course, for each choice of these parameters, the entire distribution of layer depths must be recalculated.) In this way the requirements represented by (4.11) of balance of integrated buoyancy flux through each layer determine parameters that, together with the requirements that the wind-driven circulation makes on layer depth distributions, determine the mean stratification of the ocean.

Perhaps this method of determining the stratification can be illustrated by an analogy with a simpler system. Suppose a longitudinal rod made of material of known thermal diffusivity is heated on one end at a known constant rate by electrical heating coils. We might ask, what is the eventual steady distribution of temperature in the rod? An approximate method to answer this question might consist of guessing the positions of a number of isotherms along the rod, computing the heat flux (diffusivity × temperature gradient) along the rod, comparing with the imposed heat flux, readjusting the positions of the isotherms where the agreement is worst, and repeating the process until acceptable agreement is obtained. This procedure fails if the total range of temperature in the rod is grossly underestimated in the initial guess. This manifests itself as the initial guessed heat flux being everywhere far smaller than the imposed heat flux. The remedy is plain: to choose a larger total range of temperature. Then the above procedure can be used to refine the positions of isotherms. The relevance of this simple analogy to the ocean model is obvious. The relaxation procedure is far more arduous in the ocean model because the layer topographies and circulation must be calculated for each trial setting of the layer parameters. The average thickness of layers is analogous to isotherm spacing in the rod. By the remarks about the inadequacy of the initial guessed temperature range in the rod, we anticipate a major result of this paper: that a prior choice of density range in the model ocean guided by observed density ranges from nature cannot match the buoyancy flux through the pycnocline with the surface buoyancy flux; a much larger density range is necessary.

It must be emphasized that this procedure does not jointly determine layer densities and depths, but only the latter, as long as a sufficient total range of density is allowed for.

There is a parameter, H_{j0} or y_j^w, for each layer that outcrops anywhere in the ocean basin. There is a relationship like (4.11) for each outcropping layer. Hence there are, prima facie, just enough unknown parameters and equations to determine them. However, the fact just noted, that the Nth version of (4.11) is guaranteed by specifying B_0 so that (4.12) holds and $K_{N+1} = 0$, removes the power of that equation to constrain the H_{j0}, y_j^w. This indeterminacy should be understood as follows. It has been convenient in this paper to take surface buoyancy flux B_0 as a given. In fact, there are constituents of the surface buoyancy flux, such as the sensible and latent heat fluxes, which depend on the air–sea temperature difference (Haney 1971). If this air–sea coupling of the flux constituents is taken into account, then the steady-state requirement (4.12) is not merely a constraint on an externally imposed $B_0(x, y)$ but is a true constraint on the area-average surface temperature (or density). In terms of the model, this is a constraint on the positions of the layer outcrops, and hence on the determination of the H_{j0}, y_j^w parameters. Failing such a coupling dependence in the surface flux, the one-parameter indeterminacy is simply a reflection of the fact that the thermodynamics of the system is invariant to an arbitrary shift of all the layer densities.

The $(N + 1)$th layer is put into motion by nonzero e_N [Eq. (2.7b) with $F_{N+1} = 0$]. Hence, we have calculated a layer topography $H_{N+1}(x, y)$ for this layer, given an eastern boundary value $H_{N+1,0}$. The choice of this parameter is quite arbitrary and inconsequential as this layer does not participate in the buoyancy balance (because $K_{N+1} = 0$). The depth $H_{N+1}(x, y)$ is really a proxy for the pressure distribution in the $(N + 1)$th layer.

c. *Buoyancy-driven corrections to the circulation*

In section 2 we neglected all diapycnal diffusivities $K_j = 0$. The apparent inconsistency of this with the requirements of (4.11) is resolved if the diffusive contributions to the diapycnal fluxes e_j are merely small compared to surface Ekman pumping w_{Ek}. Formally, the corrections to layer depths should be calculated from the linearized form of (2.6),

$$J\left(P_j^{(0)}, \frac{h_j^{(1)}}{f}\right) + J\left(P_j^{(1)}, \frac{h_j^{(0)}}{f}\right) = e_j^{(1)} - e_{j-1}^{(1)}, \quad (4.13)$$

where $h_j^{(1)} = H_j^{(1)} - H_{j-1}^{(1)}$, $P_j^{(1)} = \gamma_j H_j^{(1)} + \cdots + \gamma_n H_n^{(1)}$, the $H_j^{(1)}$ being the corrections to the zero-order depths $H_j^{(0)}$ obtained above. These corrections are forced on the right by the contributions to the e_j proportional to K_j; namely,

$$\gamma_j e_j^{(1)} = F_j^{(1)} - F_{j-1}^{(1)}, \quad (4.14a)$$

$$F_j^{(1)} = \frac{g}{\rho_0} K_j(\rho_{j+1} - \rho_{j-1})/2h_j^{(0)}, \quad (4.14b)$$

where zero-order thicknesses $h_j^{(0)}$ are used to estimate the diffusive fluxes. In addition to (4.13), the depth corrections must not alter the (linearized) Sverdrup balance (2.9). Hence, they must satisfy

$$\gamma_j H_j^{(0)} H_j^{(1)} + \cdots + \gamma_n H_n^{(0)} H_n^{(1)} = 0. \quad (4.15)$$

The calculation of these corrections is beyond the scope of this paper, although in the example calculations in section 5, we will obtain the corrections along the subtropical–subarctic gyre boundary so that we can show how the cross-gyre exchange, which is associated solely with the diffusive corrections, accomplishes the transport of buoyancy from subtropics to subarctic.

5. Model runs

We shall show two model runs designed to illustrate the role of buoyancy forcing in ocean circulation. In both runs we chose the following analytic form for the midocean zonal wind stress over the rectangular basin, $0 < x < a$, $-b < y < 3b$:

$$\tau^x(y) = \tau_0 \frac{f}{f_0} \xi(y) \sin\xi(y), \quad (5.1a)$$

where

$$\xi(y) = \xi_1(1 - |y - b|/2b). \quad (5.1b)$$

This gives a Sverdrup transport forcing function (2.10) of

$$\Theta = \Theta_0 \left(\frac{f}{f_0}\right)^2 \sigma^{-1}(\sin\xi + \xi\cos\xi)\epsilon(y), \quad (5.2a)$$

where $\Theta_0 = \tau_0 f_0 a \xi_1 s/\rho_0 \beta b$, and

$$\epsilon(y) = \begin{cases} -1, & y > b \\ +1, & y < b. \end{cases} \quad (5.2b)$$

The value $\xi_1 = \xi(b) = 2.029$ is chosen to be a zero of (5.2a); $\sigma = 1.391$ is the maximum value of $(\sin\xi + \xi\cos\xi)$, attained at $|y - b|/2b = 0.47$. For the zonal and meridional extent of the rectangular basin, we chose $a = 5000$ km, $4b = 6000$ km. Other physical parameters were $f_0 = 10^{-4}$ s^{-1}, $\beta = 2 \times 10^{-11}$ m^{-1} s^{-1}, $\rho_0 = 1000$ kg m^{-3}. In both runs we used $\tau_0 = 0.104$ N m^{-2} for the midocean zonal wind amplitude; this gives $\Theta_0/2f_0 = 24.5$ Sv (1 Sv $\equiv 10^6$ m^3 s^{-1}) for the approximate strength of the subtropical gyre. The Sverdrup function Θ is plotted in Fig. 4. A constant alongshore wind τ_e^y is taken to blow along the eastern boundary;[1] we set $\tau_e^y = -0.05$ N m^{-2} (equatorward). For the surface buoyancy flux, we chose

[1] This may be accomplished by adding a wind stress of the form

$$\tau' = \tau_e^y e^{-(a-x)/\lambda}(\mathbf{i} f(\beta\lambda)^{-1} \ln f + \mathbf{j})$$

to the zonal wind of Eq. (5.1a). This produces no Ekman pumping and makes no contribution to (5.2a).

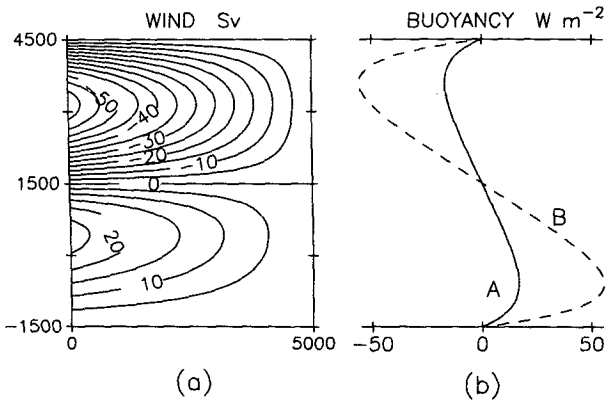

FIG. 4. (a) The Sverdrup wind forcing function $\Theta/2f_0$ used in runs A, B; units: 10^6 m^3 s^{-1}. (b) The surface buoyancy flux $c\rho B_0/\alpha g$; units: W m^{-2}. Run A (solid); run B (dashed).

$$B_0 = B_1\left(\frac{b-y}{2b}\right)(1 - e^{-(2b-|y-b|)/\lambda_B}). \quad (5.3)$$

The exponential factor (decay scale $\lambda_B = 600$ km) was introduced to bring the buoyancy forcing to zero at $y = -b$, $3b$. The buoyancy-forcing function is shown in Fig. 4b. For run A, we chose the buoyancy-forcing amplitude to be $B_1 = 1.5 \times 10^{-8}$ m^2 s^{-3}. Multiplied by the factor $\rho_0 c_p/g\alpha = (4.0 \times 10^6$ J m^{-3} °C$^{-1})/(9.8$ m s$^{-2})(2 \times 10^{-4}$ °C$^{-1}) = 2.0 \times 10^9$ J m^{-4} s^2, this is equivalent to a surface heat flux amplitude, analogous to B_1 in (5.3), of 30 W m^{-2}. (Not to be confused with the maximum surface heat flux, of 16 W m^{-2}, which occurs at $y = -598$ km.) The area-integrated equivalent heat flux into the subtropical ocean gyre ($-b < y < b$) is 0.15 PW (1 PW = 10^{15} W); a similar rate of equivalent heat transport crosses the meridional gyre boundary at $y = b$ and leaves the surface ocean in the subarctic gyre ($b < y < 3b$).

In run B, the buoyancy forcing amplitude differed from run A in being more than three times as large: $B_1 = 5 \times 10^{-8}$ m^2 s^{-3}. This is equivalent to a surface heat flux amplitude of 100 W m^{-2} (with maximum surface heat flux of 54 W m^{-2}) and an area-integrated equivalent heat flux into the subtropical ocean gyre of 0.51 PW. The wind forcing was identical to run A.

When running the model, it is necessary to select the densities of the layers. It is possible, in principle, to select a standard density difference, say $\Delta\rho = 1.0$ kg m^{-3}, and then vary the H_{j0} or y_j^w layer by layer until buoyancy balance is achieved. For a smaller choice of $\Delta\rho$ we must anticipate a larger total number of layers. Hence, to control this total number (for computational convenience we have sought to restrict it to 6 or 7), a judicious choice of $\Delta\rho$ must be made so that the total range of density required by the buoyancy balance is covered in a model with such a modest number of layers. This is arrived at by the considerations outlined in the discussion following Eq. (4.11) above.

It is not necessary or even desirable to insist on the same $\Delta\rho$ between each pair of layers; Tables 1 and 2 show the density differences and reduced gravities that have been used in runs A and B. The partitioning of the continuous density profile of the natural ocean into the discrete densities of the layered model is clearly not unique. A different choice of layer densities will lead to different topographies of layer depths. Still, by invoking the principle of consistency, that in the limit of a large number of layers with ever smaller density differences the layer equations approach the continuous isopycnal-coordinate equations of motion, we may argue that circulation solutions for particular discrete density partitions provide useful insights into natural ocean circulation.

The topographies of the depths H_j of the bases of the six layers of run A are shown in Fig. 5a. Table 1 lists the depths H_{j0} at the northeastern corner (a, b) of the subtropical gyre of the interfaces that do not outcrop in the subtropics, and the midocean outcrop latitudes y_j^w of those that do. These have been determined by the trial and error relaxation methods outlined in section 4. Also shown are the eastern boundary intersections y_j^e of the outcrop. Layer 3 carries most of the anticyclonic circulation of the subtropical gyre, deepening from 100 m along the eastern and southern boundaries, and the subtropical–subarctic boundary, to more than 600 m in the center of the gyre. Figure 6 shows the Montgomery potentials for the layers, from which the velocities may be calculated [Eqs. (2.3), (2.4)]. Layers 2 and 1 lie nested atop layer 3 in the

TABLE 1. Parameters for run A, layers 1–6. Reduced gravities γ_j, relative densities $\rho_j - \rho_1$, eastern boundary depths H_{j0}, outcrop latitudes y_j^w, y_j^e, diffusivities K_j, mean inverse thicknesses $\tilde{h}_j$, exposed surface areas A_{j-1} of waters lighter than ρ_j.

j	γ_j (m s^{-2})	$\rho_j - \rho_1$ (kg m^{-3})	H_{j0} (m)	y_j^w (km)	y_j^e (km)	K_j (10^{-4} m^2 s^{-1})	$\tilde{h}_j$ (m)	A_{j-1} (10^{12} m^2)
1	0.015	0	—	−754	−1409	—	—	—
2	0.015	1.53	—	−152	−1113	0.11	28	3.47
3	0.0135	3.06	100	—	—	1.84	230	6.61
4	0.02	4.44	700	—	—	0.69	234	15.4
5	0.02	6.48	1500	—	—	2.36	892	27.4
6	0.0075	8.52	2400	—	—	0	901	30.0

TABLE 2. Parameters for run B; similar to Table 1.

j	γ_j (m s^{-2})	$\rho_j - \rho_1$ (kg m^{-3})	H_{j0} (m)	y_j^w (km)	y_j^e (km)	K_j (10^{-4} m^2 s^{-1})	$\tilde{h}_j$ (m)	A_{j-1} (10^{12} m^2)
1	0.05	0	—	−954	−1377	—	—	—
2	0.03275	5.10	—	420	−767	0.13	37	2.55
3	0.03275	8.44	100	—	—	1.35	166	9.50
4	0.03275	11.79	500	—	—	1.15	234	15.7
5	0.025	15.13	1000	—	—	3.31	556	24.7
6	0.025	17.68	2000	—	—	0	1030	30.0

southern sector of the gyre, with maximum depths of only 60 m and 30 m, respectively. Overlaying of the Montgomery potentials shows the rightward turning of the currents with depth, as required by the beta spiral. Layer 3 outcrops very closely around the northern, eastern, and southern rim of the subarctic gyre, exposing layer 4, which is found at the surface over about three-quarters of the gyre.

Figure 5b shows the pattern of characteristics for run A of the first submerged layer in each of the regions of surface exposure of the layers. In R_3 (where layer 3 is exposed at the surface), characteristics for layer 4 start from both eastern and western boundaries. There is a stagnation point (Rossby attractor) rather close to the eastern boundary at x = 4910 km on the subtropical–subarctic gyre boundary (y = 1500 km)

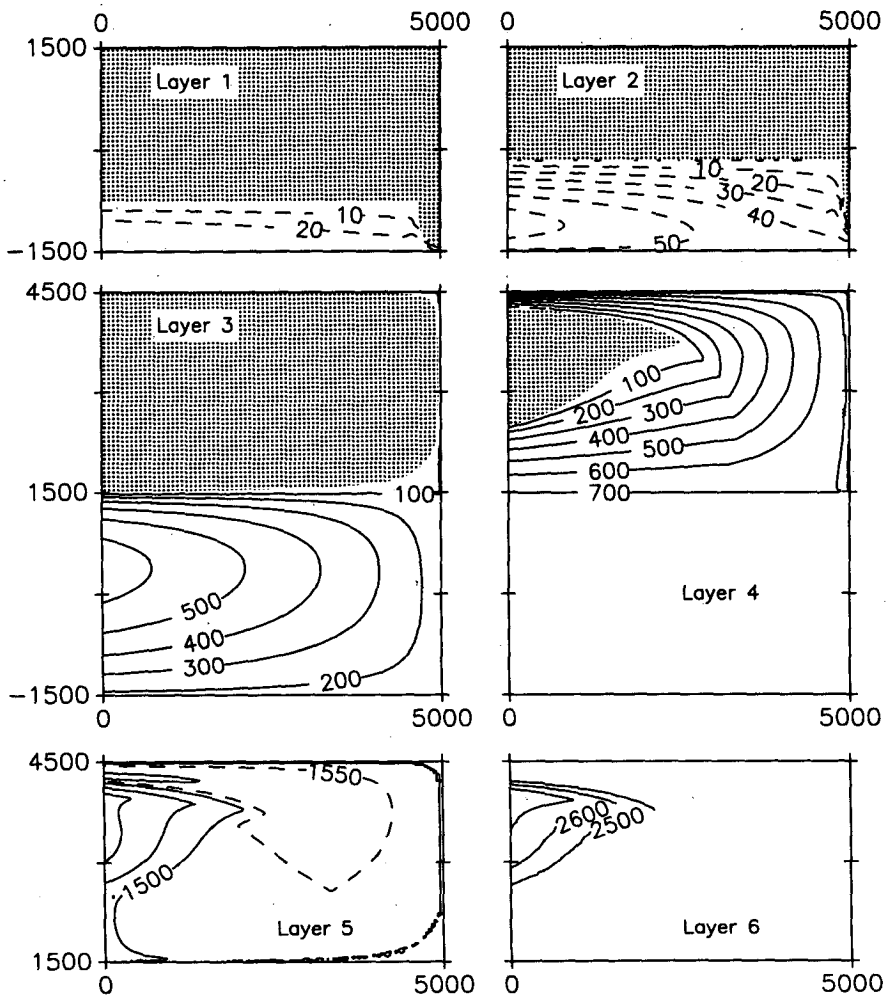

FIG. 5. (a) Depths of bases of layers 1–6 for run A. Shaded regions indicate absence of the layer. Layers 5, 6 have constant depths in the subtropics, which are not shown. (b) Characteristics of the next-to-surface layers in the various outcropping regions for run A.

from which emerge limiting characteristics, which divide R_3 into subregions reached by characteristics starting from the eastern and western boundaries (de Szoeke 1992). All characteristics return to the western boundary in the subtropics or reach the outcrop of layer 3 in the subarctic. A cusp develops in the outcrop of layer 4 in the subarctic where characteristics that originate from eastern and western boundaries near the subarctic–subtropical boundary converge. Only two layers are in motion at any given point in the subarctic: layers 3 and 4 in R_3, layers 4 and 5 in R_4, and layers 5 and 6 in R_5. Even so, the deeper of these pairs is very sluggish. The pattern of the depths of layers 4 and 5 contains most of the cyclonic circulation of the subarctic gyre.

Figures 7 and 8 show the interface depths, characteristics, and Montgomery potentials of the layers for run B. Qualitatively these figures resemble those for run A. Table 2 lists the layer densities and other parameters relevant to run B, similar to Table 1. Again, we emphasize that the depths H_{j0}, or subtropical outcrop latitudes y_j^w, have been determined by the consideration of layer buoyancy balances (section 4). The major contrast between runs A and B is the much larger density differences, two or three times larger, that have been employed in the latter. These choices were dictated by the requirement of keeping the same number of active layers (six) in the two runs.

In Tables 1, 2 we list for runs A, B the average inverse thicknesses and areas of the submerged portions of the layers, defined by

$$\tilde{h}_j = \left(\frac{1}{A_{j-1}} \int_{\substack{\cup R_k \\ k \leqslant j-1}} \frac{1}{h_j} \, dA \right)^{-1},$$

$$\text{where} \quad A_{j-1} = \int_{\substack{\cup R_k \\ k \leqslant j-1}} dA. \quad (5.4)$$

These quantities are important because they appear on the right side of Eq. (4.11), which expresses the buoyancy budget of layers lighter than the jth, and may be written

$$\int_{A_j} B_0 \, dA = \frac{g}{\rho_0} K_{j+1} \frac{\rho_{j+1} - \rho_{j-1}}{2\tilde{h}_{j+1}} A_j. \quad (5.5)$$

The $\tilde{h}_j$ are functions of "initial" interface depths H_{j0} (or outcrop latitudes y_j^w). Using these mean thicknesses, we have constructed mean density profiles for runs A, B from Tables 1, 2; these are shown in Fig. 9. Our design goal for these runs was to use diapycnal diffusivities K_j of the canonical order of magnitude 10^{-4} m^2 s^{-1} and to vary the H_{j0} (or y_j^w), while recalculating the depth topographies of the layers for each trial, until Eq. (5.5) was brought into balance. Because this procedure is rather arduous and diffusivities are in any case uncertain, we did not insist on exact balance of (5.5) for predetermined values of K_j. Instead, the K_j shown in Tables 1, 2 are the values that ensure, a posteriori, perfect balance of (5.5). Except for layer 2 in both runs, the a posteriori K_j are within a factor of 2 or so of the canonical 10^{-4} m^2 s^{-1}. For layer 2, $K_2 = 0.1 \times 10^{-4}$ m^2 s^{-1} is required for buoyancy balance. A smaller choice of ρ_3 would allow a larger K_2, and so would a more southerly choice of y_1^w, the midocean outcrop of layer 1 that partially controls the thickness of layer 2. We chose not to pursue this issue because layers 1 and 2 are so slight in thickness and play a minor role in the circulation.

The total density contrast over the six active layers of run A was 8.5 kg m^{-3}. This is larger than, though comparable to, the observed density contrast in the real ocean pycnocline. The diffusivities K_j for run B were similar to those for run A—of order 10^{-4} m^2 s^{-1} (again excepting layer 2). The total density contrast for run B was 17.7 kg m^{-3}, twice as large as for run A. Evidently, to process 0.5 PW equivalent heat flux through the system of layers of run B by satisfying the buoyancy constraints (4.11) or (5.11) requires a much stronger pycnocline than the slighter buoyancy throughput of run A. The magnitude of this density contrast is not found in the natural ocean. Even the 8.5 kg m^{-3} density contrast found necessary in run A is quite large. To reduce the density contrast in run B to, say, 5 kg m^{-3} would require diffusivities several times larger than those in Table 2.

a. Discussion

The relation between the buoyancy flux and the resulting density contrast across the pycnocline can be

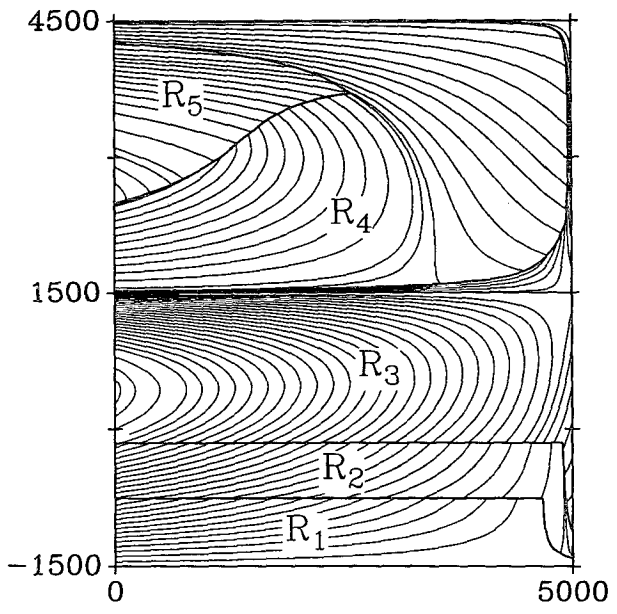

FIG. 5. (*Continued*)

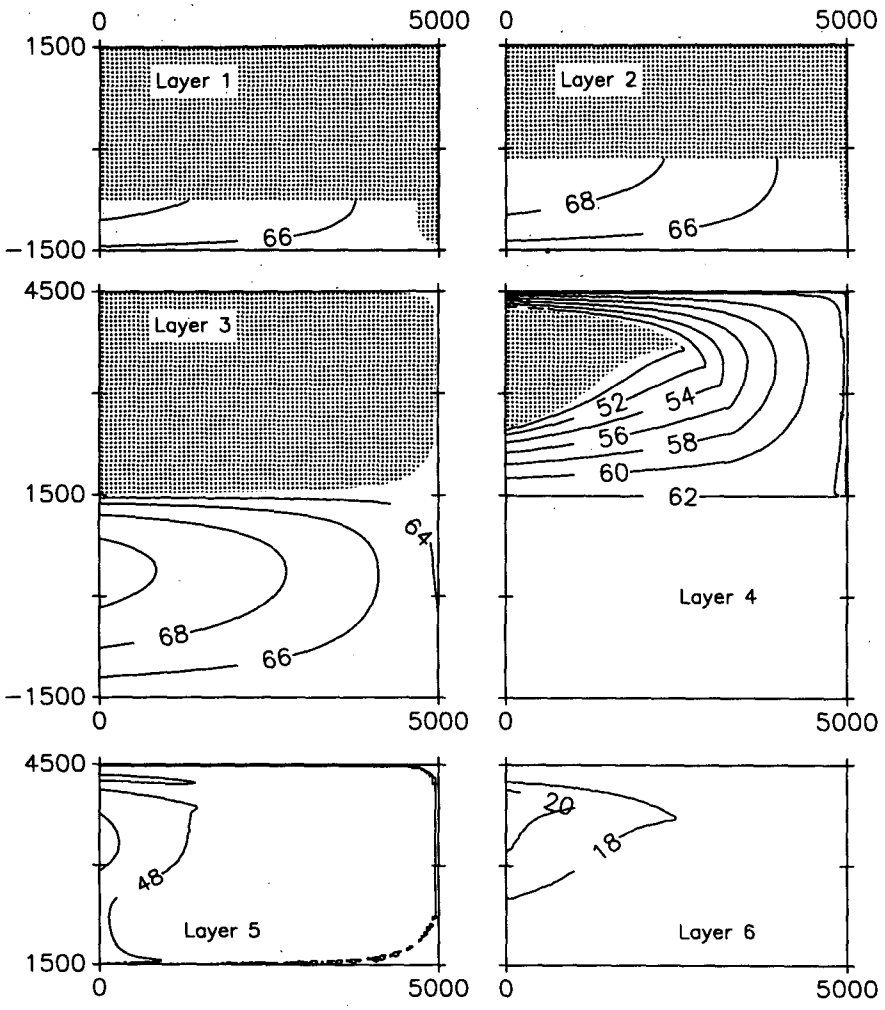

FIG. 6. Montgomery potentials of layers 1–6 for run A (unit: $m^2 s^{-2}$). Shaded regions indicate absence of the layer. Layers 5, 6 have constant potentials in the subtropics, which are not shown.

understood by a simple scaling argument. Suppose the mean surface buoyancy flux $0.34B_1$ [the factor 0.34 comes about from averaging (5.3) over the subtropics] is balanced by diapycnal diffusion across a pycnocline of thickness h_p, with density contrast $\Delta\rho_p$. This is expressed by

$$0.34B_1 \sim \frac{g}{\rho_0} K_d \frac{\Delta\rho_p}{h_p} \tag{5.6}$$

[cf. (5.5)]. For run A, the parameters $\Delta\rho_p \sim 8$ kg m^{-3}, $B_1 = 1.5 \times 10^{-8}$ $m^2 s^{-3}$, $h_p \sim 1500$ m (see Fig. 5), and $K_d \sim 10^{-4}$ $m^2 s^{-1}$ satisfy the order of magnitude balance (5.6) quite well. Similarly, for run B, the parameters $B_1 = 5 \times 10^{-8}$ $m^2 s^{-3}$, $\Delta\rho_p \sim 18$ kg m^{-3}, with $K_d \sim 10^{-4}$ $m^2 s^{-1}$, and $h_p \sim 1200$ m satisfy (5.6). Equation (5.6) illustrates the link between diapycnal diffusivity, density gradient, and surface buoyancy flux. Given a canonical diffusivity of 10^{-4} $m^2 s^{-1}$ [which can scarcely be exceeded if microstructure measurements are to be believed (Gregg 1987)], sustaining an average surface buoyancy flux of 0.5×10^{-8} $m^2 s^{-3}$ in the subtropics requires a density gradient through the main pycnocline about twice as large as is observed (run A). This buoyancy flux is equivalent to an average heat flux of 10 W m^{-2} and drives an equivalent meridional heat transport of 0.15 PW into the subarctic gyre. Substantially larger average surface buoyancy fluxes, such as in run B, which are equivalent to meridional heat transports of about 0.5 PW into the subarctic, require density gradients across the pycnocline many times larger than observed. Substantially larger diapycnal diffusivities than $O(10^{-4}$ $m^2 s^{-1})$, combined with reasonable density gradients, could satisfy (5.6), but these seem very difficult to reconcile with microstructure observations (Gregg 1987). Indeed, diapycnal diffusivities rather smaller than this, about 0.1×10^{-4} $m^2 s^{-1}$,

have been estimated from dye release experiments in the ocean (Ledwell et al. 1993).

Our model does not include a representation of the western boundary current. One might object that the neglect of the western boundary introduces a serious error into the calculation of the right side of the buoyancy balance (4.11) on two possible grounds: mean density layer thicknesses in the boundary current may become smaller; diapycnal diffusivities in the boundary current ought to be larger because of higher currents and current shears. On the first point, pycnoclines do intensify (isopycnal spacing becomes thinner) as they rise near the western boundary, but an inspection of ocean sections suggests that perhaps isopycnal spacing in the boundary current is half what it is in the open ocean. For the second point, quantitative information about diffusivities in western boundary currents is sparse, though what there is does not support larger diffusivities (Winkel et al. 1992). In any case western boundary currents occupy less than 5% of the ocean area. For the contribution of the western boundary region to (4.11) to be significant, diapycnal diffusivities at least an order of magnitude larger than the canonical midocean value, 10^{-4} m^2 s^{-2}, would be required.

The present model runs may be compared to Bryan's (1987) calculations of ocean circulation and heat flux using the Bryan–Cox primitive equation model (Cox 1984). Bryan (1987) explored the sensitivity of this model to vertical and horizontal eddy diffusivities of heat K_{HV}, K_{HH}. It must be emphasized that the effective *diathermal* (i.e., across isotherms) eddy diffusivity in such models is, as Redi (1982) and McDougall and Church (1986) make clear,

$$K_d = K_{HV} + K_{HH}|\nabla z_T|^2,$$

where ∇z_T is the slope of isotherms. Bryan (1987) shows a calculation (his experiment 1) in which $K_{HV} = 0.5 \times 10^{-4}$ m^2 s^{-1}, $K_{HH} = 1.0 \times 10^3$ m^2 s^{-1}, and the surface heating is such that the poleward heat transport across 45°N, the subtropical gyre boundary, is 0.4 PW. The 10°C isotherm outcrops along 45°N, approximately. Estimating an average $(\partial T/\partial z)_{10°C} \sim 0.025$ C m^{-1}, from Bryan's (1987) published model cross section, over the submerged area of the 10°C isotherm, 5000 km × 6000 km = 3×10^{13} m^2, one obtains for the flux across 10°C, in the interior portion away from the western boundary current, where $|\nabla z_T| \ll 10^{-5}$, $K_d \approx K_{HV}$,

$$F_{\text{interior}} = (\rho c K_{HV} \partial T/\partial z)(\text{area}) = 0.15 \times 10^{15} \text{ W}.$$

This is substantially too small to account for the transport across 45°N. However, in the boundary current, where $|\nabla z_T| \approx 10^{-3}$, K_d is dominated by the second term, which is about 20 times larger than K_{HV}

$$(K_d)_{\text{WBC}} \approx K_{HH}|\nabla z_T|^2 \approx 10 \times 10^{-4} \text{ m}^2 \text{ s}^{-1}.$$

Hence, the flux of heat through the isotherm in the western boundary current is

$$F_{\text{WBC}} \approx \rho c K_d \frac{\partial T}{\partial z} A_{\text{WBC}} = 0.19 \times 10^{15} \text{ W},$$

where we used $A_{\text{WBC}} \approx 2 \times 10^{12}$ m^2. The sum of F_{interior} and F_{WBC} then substantially accounts for Bryan's poleward heat transport across 45°N. Yet it must be emphasized that the major contributor is F_{WBC}, which is entirely due to the form of parameterization of diffusion processes in the model. This is precisely the situation of which Veronis (1975), Redi (1982), and McDougall and Church (1986) warned. There seems to be little observational basis for accepting an effective diathermal diffusivity as high as 10×10^{-4} m^2 s^{-1} (Gregg 1987; Winkel et al. 1992), even in western boundary current regions. Bryan (1987) shows another run (experiment 4), with $K_{HV} = 2.5 \times 10^{-4}$ m^2 s^{-1}, $K_{HH} = 1.0 \times 10^3$ m^2 s^{-1}, in which a poleward heat transport of 1.0 PW across 45°N is achieved. Again, the greater portion of the net diathermal heat transport across the 10°C isotherm (which again outcrops at about 45°N) takes place in the western boundary current with effective diathermal diffusivities of

$$(K_d)_{\text{WBC}} \approx K_{HH}|\nabla z_T|^2 \sim 40 \times 10^{-4} \text{ m}^2 \text{ s}^{-1}.$$

The same objections to such a high diffusivity may be made.

The final point to be made in comparing Bryan's (1987) runs to ours is that his subtropical gyre area was about twice as large as in our runs. This is an important factor in comparing runs since the heat transports are expected to scale with the area. Hence, our run A (equivalent poleward heat transport = 0.15 PW) is comparable to Bryan's experiment 1 (0.4 PW), and run B (0.51 PW) to experiment 4 (1.0 PW).

It is worth emphasizing that the shortcomings of the buoyancy cycle in Bryan's (1987) coarse-resolution model cannot be amended with a parameterization of alongisopycnal buoyancy transport by mesoscale eddies, such as proposed by Gent and McWilliams (1990). The essential difficulty in ocean models with diapycnal diffusivity coefficients of order 10^{-4} m^2 s^{-1} is their inability to get buoyancy across isopycnals; redistributing buoyancy along isopycnals does not resolve the difficulty.

b. *Layer transports across the subtropical–subarctic boundary*

We shall calculate the way in which volume and buoyancy are transported across the subtropical–subarctic gyre boundary. In the absence of buoyancy forcing and diapycnal diffusion, there is no mass exchange across the subtropical–subarctic boundary, either in the interior or the western boundary current, in any layer. Given buoyancy forcing and diffusion, the pointwise vertical exchanges of mass, layer by layer, can be cal-

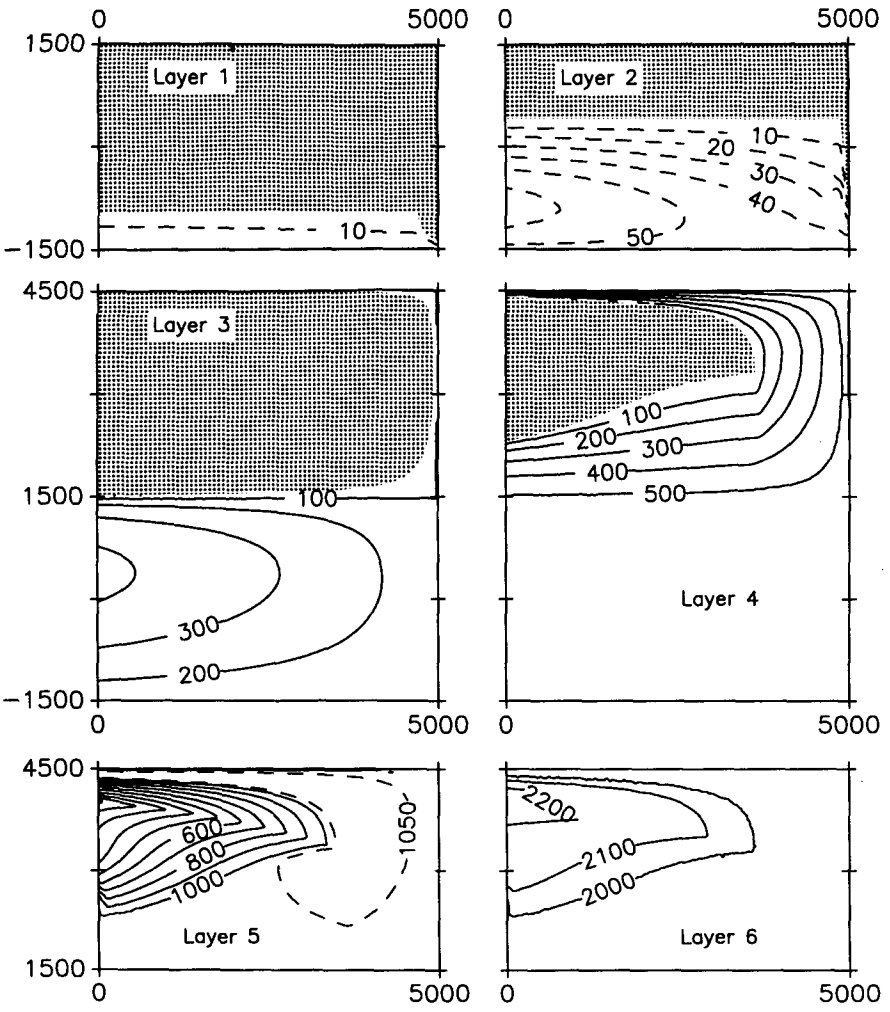

FIG. 7. (a) Depths of layer bases and (b) characteristics for run B, similar to Fig. 5.

culated from (2.7b–d). Integrating these over the subtropics gives the required layer by layer exchange across the boundary with the subarctic.

Run A. For example, we can calculate the area-mean diapycnal fluxes $\bar{F}_4, \bar{F}_5$ from the average inverse thicknesses of layers 4 and 5 in the subtropical gyre ($0 < x < a$, $-b < y < b$; see Fig. 5), and the diffusivities K_4, K_5 from Table 1, using (2.7d). In this way, we obtain $\bar{F}_4 = 0.50 \times 10^{-8}$ m^2 s^{-3}, $\bar{F}_5 = 0.59 \times 10^{-8}$ m^2 s^{-3}. Since the integral of the buoyancy flux through layer 3 over the subtropics must equal the surface buoyancy flux over the subtropics, it is easy to calculate $\bar{F}_3 = \int_{ST} B_0 dA/A_{ST} = 0.51 \times 10^{-8}$ m^2 s^{-3} from (5.3). These three fluxes are nearly the same. By hypothesis, the vertical flux through layer 6, which never outcrops in the subtropics or subarctic, is zero, $F_6 = 0$. From these mean fluxes the average entrainment velocities across the various interfaces may be calculated from Eq. (2.7c): $\bar{e}_3 = 0.6 \times 10^{-8}$ m s^{-1}, $\bar{e}_4 = -4.5 \times 10^{-8}$ m s^{-1}, $\bar{e}_5 = 0.30 \times 10^{-6}$ m s^{-1}, $e_6 = 0$. The first two of these $\bar{e}_3$, $\bar{e}_4$, are so small because of the near cancellation of $\bar{F}_3, \bar{F}_4, \bar{F}_5$ in (2.7c). The transport of layer j across the subtropical–subarctic gyre boundary, $y = b$, is given by

$$T_j = (\bar{e}_j - \bar{e}_{j-1})A_{ST}, \tag{5.7}$$

where $A_{ST} = 15 \times 10^{12}$ m^2 is the area of the subtropics. (For $j = 3$, simply take $\bar{e}_2 = 0$.) From this formula we obtain $T_3 = 0.1$ Sv, $T_4 = -0.8$ Sv, $T_5 = 5.1$ Sv, $T_6 = -4.4$ Sv. These add to zero, as they must. The first two of these are small because of the smallness of $\bar{e}_3$, $\bar{e}_4$. This is connected with the outcropping of the bases of layers 3 and 4 in the subarctic gyre in such a way that the net buoyancy loss from the two layers is quite small. Because of this, very little mass exchange in the two layers across the subarctic–subtropical boundary is required. However, the buoyancy gained by the ocean in the subtropics must migrate across these layers, eventually to be given up at the surface in the subarctic by denser layers. This is the reason for the close identity

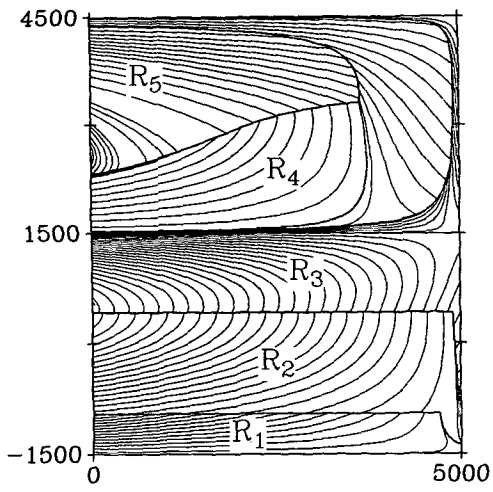

FIG. 7. (*Continued*)

of $\bar{F}_3, \bar{F}_4, \bar{F}_5$. The net buoyancy transport across $y = b$ is given by

$$\gamma_6 T_6 + (\gamma_6 + \gamma_5)T_5 + (\gamma_6 + \gamma_5 + \gamma_4)T_4 + (\gamma_6 + \gamma_5 + \gamma_4 + \gamma_3)T_3 = 7.6 \times 10^4 \text{ m}^4 \text{ s}^{-3}, \quad (5.8)$$

which matches $\int_{ST} B_0 dA$, as required. If the buoyancy was due solely to temperature, this buoyancy transport would be equivalent to 0.15 PW. The buoyancy transport across the subtropical–subarctic boundary is accomplished principally by the exchange of about 5 Sv of layers 5 and 6 water, with a small modification due to southward transport of about 0.8 Sv of layer 4 water. The relationships of the horizontally averaged buoyancy fluxes, the averaged layer-interface entrainments, and the volume transports across the subtropical–subarctic boundary are shown in a schematic meridional section in Fig. 10a.

The layer volume transports just quoted at the subtropical–subarctic boundary are the totals for each layer: the geostrophic interior transport plus western boundary current transport. While the theory does not take explicit account of the dynamical mechanisms of the boundary current, we can calculate the geostrophic transport in each layer in the ocean interior and the required compensating boundary current transport by subtraction. At lowest order, that is, neglecting all diapycnal diffusivities, $K_j = 0$, there is no meridional geostrophic motion across $y = b$ in any layer. Layer 3, in contact with the surface wind, carries −9.5 Sv (equatorward) in its Ekman layer. Presumably, a like amount is carried poleward in this layer in its western boundary current. This lowest-order view of the circulation across the subtropical–subarctic boundary cannot account for the necessary exchange of buoyancy. We will consider the modifications to this picture at first order in K_j that are necessary to bring the circulation system into buoyancy balance.

The lowest-order Montgomery pressures $P_4^{(0)}$, $P_5^{(0)}$, $P_6^{(0)}$ are constant along, and to the south of, $y = b$. Hence, Eq. (2.6) may be approximated by

$$\partial_x P_j^{(1)} \partial_y \frac{h_j^{(0)}}{f} = e_j^{(1)} - e_{j-1}^{(1)} \quad (5.9)$$

for $j = 4, 5, 6$, where the (0) superscripts refer to fields computed by neglecting the diffusivities K_j, and the (1) superscripts refer to first-order fields computed by taking the K_j into account. In particular the $e_j^{(1)}$ on the right of (5.9) are given by

$$\gamma_j e_j^{(1)} = F_j^{(1)} - F_{j+1}^{(1)}, \quad (5.10)$$

where

$$F_j^{(1)} = K_j \frac{\frac{1}{2}(\gamma_j + \gamma_{j-1})}{h_j^{(0)}}, \quad j > 3 \quad (5.11a)$$

$$0, \quad j = 3. \quad (5.11b)$$

The $h_j^{(0)}$ are $h_6^{(0)} = 2400 - 1500 = 900$ m, $h_5^{(0)} = 1500 - 700 = 800$ m, and $h_4^{(0)} = 700 - 100 = 600$ m. They are constant along $y = b$. Hence, $F_6^{(1)} = 0$ (by hypothesis), $F_5^{(1)} = 0.59 \times 10^{-8}$ m^2 s^{-3}, $F_4^{(1)} = 0.19 \times 10^{-8}$ m^2 s^{-3}, and $e_6^{(1)} = 0$, $e_5^{(1)} = 0.30 \times 10^{-6}$ m s^{-1}, $e_4^{(1)} = -0.20 \times 10^{-6}$ m s^{-1}, $e_3^{(1)} = -0.14 \times 10^{-6}$ m s^{-1}. The entrainment velocities $e_3^{(1)}$, $e_4^{(1)}$ along $y = b$ need not be the same as the averages $\bar{e}_3$, $\bar{e}_4$ over the subtropics. Equation (5.9) may be integrated from east to west along $y = b$, assuming $P_j^{(1)}(a, b) = 0$, to obtain $P_j^{(1)}(x, b)$. Clearly, the $P_j^{(1)}$ will be linear functions of x. The same linear relation (2.3) holds between the first-order corrections $P_j^{(1)}$ and $H_j^{(1)}$ as holds for the total fields P_j and H_j. Hence, the changes in H_j caused by the first-order entrainments can be calculated. The results are shown schematically in Fig. 10b: H_6 shoals from east to west from 2400 to 2215 m, H_5 deepens from 1500 to 1700 m, and H_4 shoals from 700 to 549 m. The layer-3 depths ought to be recalculated from (2.9) (with $n = 6$, $k = 3$). Unfortunately, this leads to absurd (imaginary!) depths for H_3 beginning not far out from the eastern boundary. This is merely a sign of the southward reorientation of the position of the outcrop line $H_3 = 0$ of layer 3, whose lowest-order position in the subarctic is quite close to $y = b$ (Fig. 5). This reorientation is made necessary by the nonzero $e_j^{(1)}$. (The recalculation of the surface outcrops is beyond the scope of this paper.) The meridional transport of layer 5 in the geostrophic interior is

$$\int_0^a (H_6 - H_5) f^{-1} (\partial P_6 / \partial x) dx.$$

Because H_6, P_6, etc., vary linearly in x across the geostrophic interior, this integral is simply

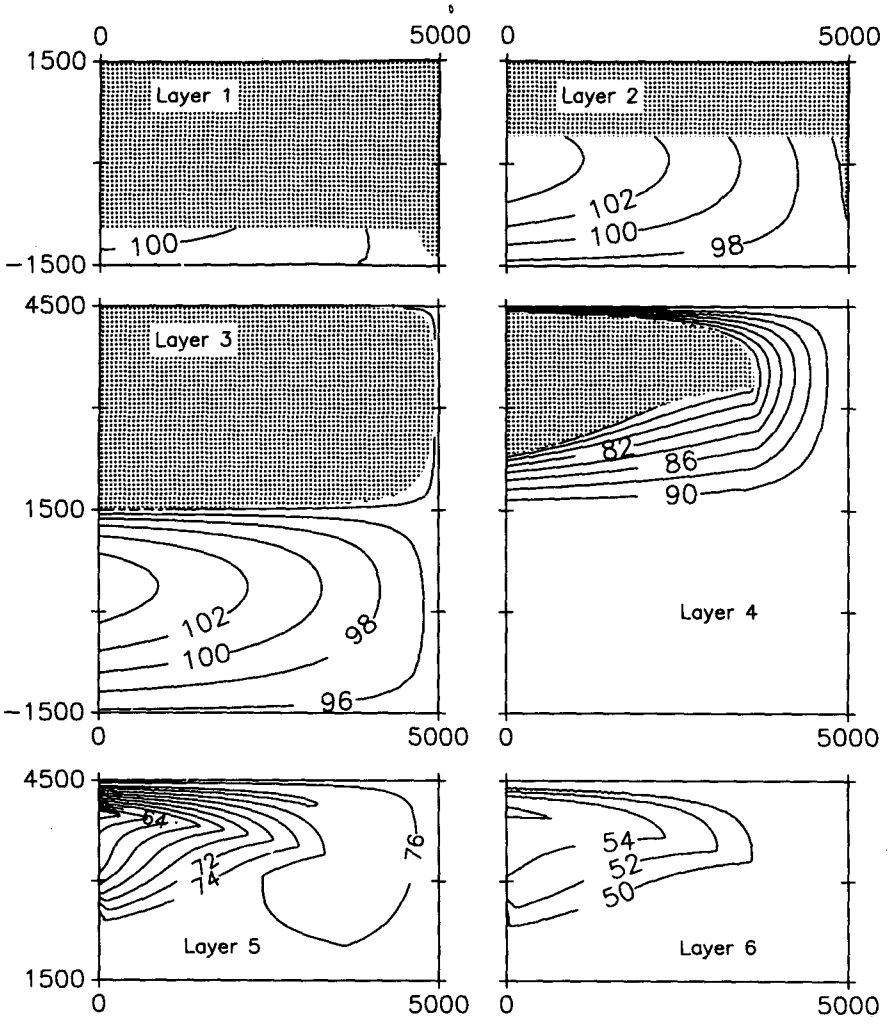

FIG. 8. Montgomery potentials for run B, similar to Fig. 6.

$$\frac{1}{2}\{(H_6 - H_5)_{x=0} + (H_6 - H_5)_{x=a}\} f^{-1} \Delta P_6$$

and may be very readily calculated to be 7.6 Sv (poleward). To restore the total meridional transport calculated above for layer 6, −4.4 Sv, a western boundary current transport of −12.0 Sv (equatorward) is required. A similar calculation of the meridional interior geostrophic transport across $y = b$ in layer 5 gives −19.6 Sv (equatorward). To restore a total of 5.1 Sv requires a western boundary current transport of 24.7 Sv (poleward) in layer 5. For layer 4, the meridional interior geostrophic transport across $y = b$ is −2.4 Sv (assuming that layer-3 thickness goes to zero in the west). Returning the −0.8 Sv total for layer 4 requires a western boundary current transport of 1.6 Sv. We have not attempted to calculate transports for layer 3 because it evidently vanishes at some point across the section.

Run B. A similar calculation of the layer transports across the subtropical–subarctic boundary can be done for run B. The mean vertical buoyancy fluxes through the layers in the subtropics are $F_6 = 0$, $F_5 = 1.91 \times 10^{-8}$ m^2 s^{-3}, $\bar{F}_4 = 1.61 \times 10^{-8}$ m^2 s^{-3}, $\bar{F}_3 = 1.70 \times 10^{-8}$ m^2 s^{-3}, calculated by means similar to run A. The average entrainment velocities across the layer interfaces are then [Eq. (2.7c)] $\bar{e}_3 = 0.03 \times 10^{-6}$ m s^{-1}, $\bar{e}_4 = -0.09 \times 10^{-6}$ m s^{-1}, $e_5 = 0.76 \times 10^{-6}$ m s^{-1}, $e_6 = 0$. Hence, the total transports of the layers across the subtropical–subarctic gyre boundary are $T_3 = 0.4$ Sv, $T_4 = -1.8$ Sv, $T_5 = 12.9$ Sv, $T_6 = -11.5$ Sv. As in run A, $\bar{F}_3$, $\bar{F}_4$, $\bar{F}_5$ are very similar, so that $\bar{e}_3$, $\bar{e}_4$ are quite small, as are the subtropic–subarctic meridional transports T_3, T_4. The buoyancy gained at the surface in the subtropics crosses layers 3 and 4 and is given up in the subarctic by layer 5. The net buoyancy transport across the gyre boundary, calculated by substituting in the left side of (5.8), is 2.55×10^5 m^4 s^{-3}, the same as $\int_{ST} B_0 dA$. This is equivalent to a heat transport of 0.51 PW. Layers 5 and 6 are primarily

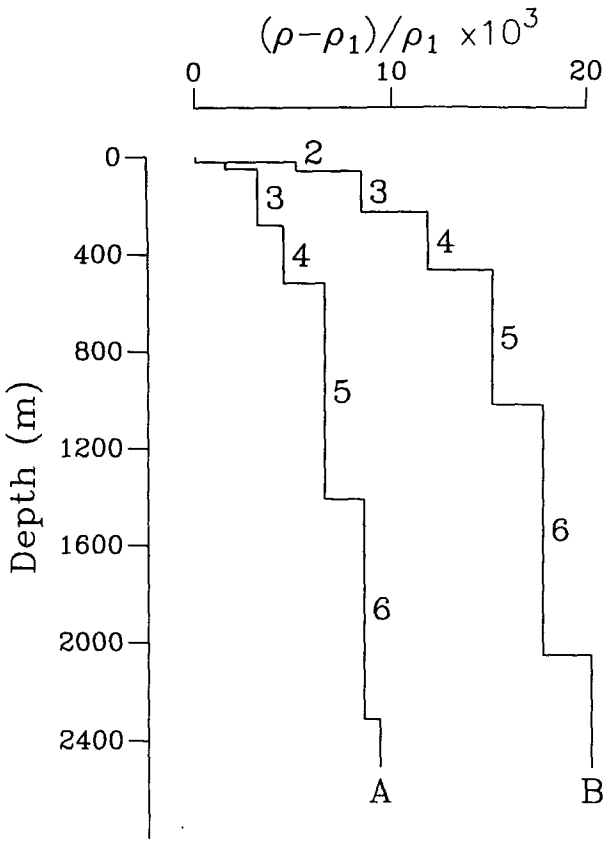

FIG. 9. Density profiles for runs A, B constructed from the average submerged thicknesses in Tables 1, 2.

responsible for exchanging buoyancy across the gyre boundary. The situation is summarized in the schematic meridional section across the subtropical gyre shown in Fig. 11a.

The changes in the interface depths H_j caused by the diffusion-driven entrainments along the subtropical–subarctic gyre boundary can be calculated by the same method used for run A. This shows that H_6 shoals from 2000 m at the eastern boundary to 1950 m in the west, just outside the western boundary current; H_5 deepens from 1000 m in the east to 1113 m; and H_4 deepens from 500 m in the east to 598 m. Again the corrections to H_3 cause it to shoal to zero along the gyre boundary, signaling a southward repositioning of the outcrop line, where $H_3 = 0$, of layer 3, whose lowest-order position is quite close to the gyre boundary. A schematic zonal section along the subtropical–subarctic boundary is shown in Fig. 11b, illustrating the perturbed layer-interface positions. The figure also shows the meridional volume transports in the interior of each layer (excluding the western boundary current), which can be calculated by the same method described above for run A, and the required compensating western boundary current transports in each layer.

Comparing runs A and B, we see that the same layers (5 and 6) are primarily responsible for the buoyancy exchange across the subtropic–subarctic gyre boundary (Figs. 10a, 11a), although the volume transports for run B are more than twice as large [the reduced gravities between the two layers are comparable: 0.02 m s^{-2} (run A), 0.025 m s^{-2} (run B)]. The product of volume transport and reduced gravity accounts for the tripling of buoyancy transport between run A and run B. The partitioning within a layer of its total meridional transport between western boundary current and geostrophic interior shows no particular pattern (Figs. 10b, 11b) though individual magnitudes up to 25 Sv are seen. In run A, the western boundary current transports 14.3 Sv poleward across the subtropical–subarctic boundary, with an equal and opposite return in the interior. In run B, the boundary current transports 19.7 Sv poleward.

The model ocean of run B, carrying buoyancy across the subarctic–subtropical boundary at an equivalent heat flux rate of 0.5 PW, requires very large density differences across the layers (numbers 3, 4, 5, and 6) involved in the transfer, given a diapycnal diffusivity of order 10^{-4} m^2 s^{-1}. Such large density differences would not be required if a more vigorous mixing mechanism, giving a much larger effective diapycnal diffusivity, were available. A leading candidate for such a role would be mixing in the upper ocean, caused by a combination of wind stirring and buoyant convection, in which effective diapycnal diffusion coefficients several orders of magnitude larger than 10^{-4} m^2 s^{-1} can be episodically but reliably achieved. In terms of run B, if such a mixing mechanism could be built into the model, the necessity for large density differences between layers 3, 4, 5 necessary to sustain large diapycnal buoyancy fluxes, could be short circuited by large diapycnal exchanges where the bases of these layers come close to the ocean surface.

6. Concluding remarks

A model consisting of discrete density layers, some of which outcrop at the ocean surface, was developed to compute the stratified ocean circulation driven by surface wind stress and buoyancy flux. At lowest order, only the Ekman pumping and surface buoyancy flux drive the surface and next-to-surface layers, while deeper layers conserve potential vorticity. At higher order, the buoyancy budgets of the layers cannot be balanced without considering diapycnal diffusion through the deeper layers. The requirements of buoyancy balance were used to determine parameters, such as layer-interface outcrop latitudes, or interface depths along the eastern boundary, which determine the mean stratification of the ocean for a given integrated surface buoyancy throughput. Two idealized runs were shown. In both runs an identical wind stress pat-

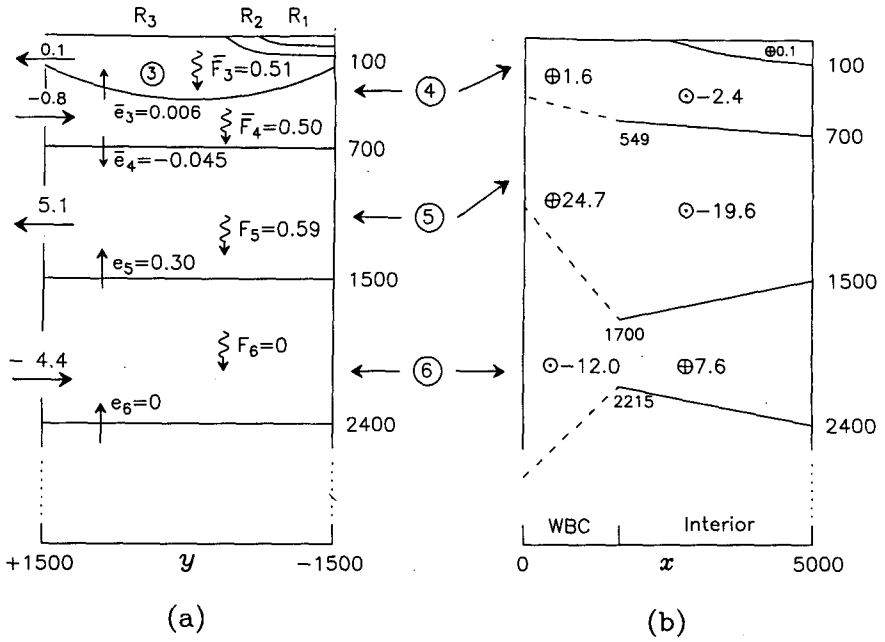

FIG. 10. (a) Schematic meridional section across the subtropics showing zero-order layer depths, buoyancy flows F_j (unit: 10^{-8} m^2 s^{-3}), layer interface entrainment velocities e_j (unit: 10^{-6} m s^{-1}), and meridional volume transports (Sv) across the subtropical–subarctic boundary. (b) Schematic zonal section along the subtropical–subarctic boundary showing first-order variations of layer depths and partition of volume transports among the western boundary current and geostrophic interior: run A.

tern and magnitude was imposed, which drove an anticyclonic gyre in the subtropics and a cyclonic gyre in the subarctic. Buoyancy forcing was positive (equivalent to heating) in the subtropics, negative (cooling) in the subarctic, but differed in magnitude between the two runs, giving a poleward buoyancy

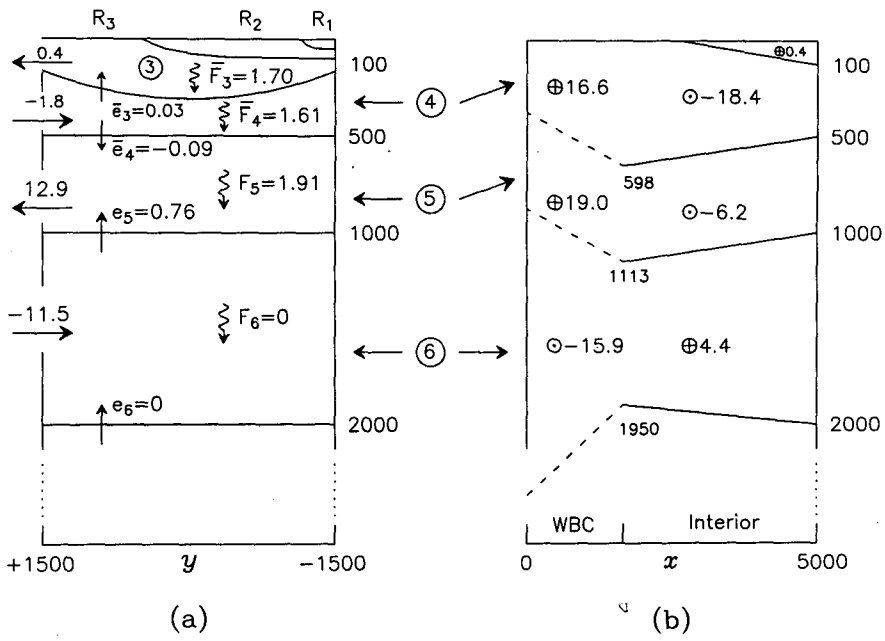

FIG. 11. As in Fig. 10: run B.

transport across the subtropical–subarctic boundary of 7.6×10^4 m^4 s^{-3} (equivalent to a poleward heat transport of 0.15 PW) in one case, and 2.55×10^5 m^4 s^{-3} (equivalent to 0.51 PW) in the other. By insisting on diapycnal diffusivities no larger than O(10^{-4} m^2 s^{-1}) we found that density contrasts of 8 kg m^{-3} and 18 kg m^{-3} across the pycnocline, respectively, were required in the two cases. A simple scaling argument based on buoyancy balance [Eq. (5.6)] confirms these magnitudes and shows the link between diapycnal diffusivity and density gradient in the pycnocline, and buoyancy throughput.

It is very disquieting that such large density gradients—giving far larger density contrasts than are observed in nature—are required to accomplish an equivalent heat throughput of O(1 PW). Meridional oceanic heat transports of such a magnitude have been computed from budgets of air–sea heat exchange (Sellers 1965), as a residual of the atmospheric heat budget (Carissimo et al. 1985), and from direct estimates based on oceanographic measurements (Bryan 1962; Bennett 1978; Bryden and Hall 1980). Speer and Tziperman (1992) calculated the so-called watermass transformation function, the transport of buoyancy across the area of ocean surface contained within a density increment about a particular contour of surface density, from climatological compilations of air–sea heat and freshwater exchanges, and displayed it as a function of density. The left side of (4.11) is the integral of surface buoyancy flux over all surface waters lighter than ρ_j. In the continuous limit, it is the integral with respect to density of Speer and Tziperman's (1992) water mass transformation function and must be related, according to (4.11), to the diapycnal buoyancy flux across the submerged isopycnal surface ρ_j. Parameterizing diapycnal buoyancy flux by the continuous analog of (2.7d),

$$\frac{g}{\rho_0} K_d \partial\rho/\partial z,$$

one may readily confirm from Speer and Tziperman's (1992) figures, and from reasonable estimates of $\partial\rho/\partial z$, that the buoyancy balance (4.11) cannot be achieved with diffusivities K_d of order 10^{-4} m^2 s^{-1}.

Microstructure measurements of turbulence in the ocean, from which estimates of diapycnal buoyancy flux (actually diathermal heat flux) and diffusivity may be made, have been accumulating in recent years. Gregg (1987) has written a very useful review of this field. The turbulence measurements give no support for mean diffusivities larger than O(10^{-4} m^2 s^{-1}); if anything, rather smaller estimates are consistently indicated. Numerical models of ocean circulation such as Bryan's (1987) do achieve meridional heat transport as large as 1 PW, but analysis suggests that much of the required diathermal heat flux is achieved in the western boundary current where, as Redi (1982) and McDougall and Church (1986) point out, fictitiously high effective diathermal diffusivities, perhaps up to two orders of magnitude larger that 10^{-4} m^2 s^{-1}, can occur because of the strong tilting of isotherms and the assumed form of the horizontal diffusivity.

The suggestion inferred from such models that much of the diapycnal (diathermal) reprocessing of buoyancy (heat) takes place in the western boundary currents may well be correct. However, it is germane to point out that the required order of magnitude of diapycnal diffusivity remains to be observed (Gregg 1987). Perhaps this is due to a lack of turbulence measurements, because of overwhelming practical difficulties, in the highly energetic layers of the western boundary currents (but see Winkel et al. 1992). It is certainly troubling that models are based on parameterizations of diffusive transport that lack observational support or even contradict it.

Western boundary currents, the regions near them, and their extensions into the midocean where they separate from the boundary are regions of intense mesoscale eddy activity. Can mesoscale eddies bring about some diapycnal mixing? We have emphasized in the derivation of the layered equations (section 2) that the layer interfaces of the discrete model are analogs of isopycnal surfaces that we take to be constructed from density fields averaged only over small-scale microstructure processes (Gent and McWilliams 1990; de Szoeke and Bennett 1993). Further averaging on fluctuating isopycnal surfaces over mesoscale variability produces no further diapycnal exchanges. The price for taking this approach to averaging the momentum and thermodynamic equations is the appearance of an extra term $-\overline{h'\nabla p'}/\rho_0\bar{h}$, due to thickness–pressure gradient correlation, in the momentum equations in addition to terms similar to the usual Reynolds stress divergence. While de Szoeke and Bennett (1993) suggest that this term is negligible, this may not be so in high-eddy regions. Then this term may drive an enhancement of the effective layer transport velocity. Gent and McWilliams (1990) propose a parameterization of this mesoscale enhancement that, whatever its other merits, produces no diapycnal flow and cannot reconcile the difficulty of achieving the necessary diapycnal buoyancy flux in the pycnocline to balance the surface sources.

How else could O(1 PW) meridional heat transports be accomplished in the ocean? In other words, how can integrated surface buoyancy flux of order 0.5×10^6 m^4 s^{-3} (equivalent to 1 PW) into waters lighter than a certain density be carried across the corresponding submerged isopycnal in order to satisfy the equilibrium buoyancy balance (4.11)? In the North Atlantic, Speer and Tziperman (1992) found an integrated surface buoyancy flux [$-g\rho^{-1}\int^{\rho} F(\rho')d\rho'$ in their notation] of this magnitude in waters lighter than σ = 23.25

kg m^{-3}. This isopycnal is found at quite shallow depths in the subtropical North Atlantic, say above 150 m. Hence, it is likely that far more vigorous mixing processes, driven from the surface by wind stirring and convection and able to attain very large effective diffusivities, are responsible for the diapycnal buoyancy flux required for balance on the right side of (4.11). This seems to imply that the buoyancy pathways in the ocean are confined to quite shallow depths in the pycnocline.

Acknowledgments. I have benefitted from discussions with A. Bennett and T. Dillon. The work was supported by NSF Grant OCE-8901187, NASA Grant NAGW-1883, and ONR Grant N00014-90-J-1133.

APPENDIX A

Ekman Layer Buoyancy Advection

The total downward buoyancy flux at the ocean surface is (Gill 1982)

$$B_0 = g\alpha Q_0/\rho_0 c_p + g\beta S_0(P - E), \qquad \text{(A1)}$$

where Q_0 is the total downward heat flux (W m^{-2}) at the ocean surface, and P, E are precipitation and evaporation rates (m s^{-1}), $\alpha = -\rho^{-1}\partial\rho/\partial T$ is thermal expansibility of seawater, $\beta = \rho^{-1}\partial\rho/\partial S$ is saline expansibility, c_p is specific heat of seawater, and S_0 is mean surface salinity. The modified buoyancy flux B_0', which appears in the definition of e_k [Eq. (2.7b)], and hence in the circulation equation (2.22), is given by

$$B_0'(x, y) = B_0(x, y) + \sum_j \gamma_j E_j \tilde{u}_j(x, y), \qquad \text{(A2)}$$

where

$$E_j = -\int_{Y_j} (\rho_0 f)^{-1}\boldsymbol{\tau}\cdot d\mathbf{l} \qquad \text{(A3)}$$

is the total Ekman transport across the jth outcrop $y = Y_j(x)$. The sum in (A2) is taken over all outcropping interfaces. The correction term in (A2) is necessary to account for the change in density of water being pushed across outcrops by the ageostrophic Ekman transport; the buoyancy source for this density modification is subtracted from the surface buoyancy flux B_0. The shape function $\tilde{u}_j(x, y)$ distributes this subtraction over a region in the vicinity of $Y_j(x)$; it must satisfy the normalization condition

$$\int \tilde{u}_j(x, y)dA = 1, \qquad \text{(A4)}$$

where the integration is taken over the entire domain of the ocean. For outcrops in the subtropical gyre we chose $\tilde{u}_j$ so that

$$\int_{R_j} \tilde{u}_j dA = 1 \quad \text{(subtropics)}, \qquad \text{(A5)}$$

where R_j is the region where layer j is in contact with the surface, and $\tilde{u}_j$ is identically zero outside R_j. The interpretation of such a shape function in (A2) is that the buoyancy necessary to change water of density ρ_{j+1} flowing south in the Ekman layer across the jth outcrop into density ρ_j should be subtracted from the surface buoyancy flux in region R_j, and the remainder B_0' applied to modifying the density of water entrained across the submerged part of the jth interface at the rate e_j given by (2.7b,c). Nurser and Marshall (1991) introduced a similar Ekman transport correction to the surface buoyancy flux in a continuous theory of the interaction between the mixed layer and the thermocline.

For outcrops in the subarctic gyre, it is more convenient to choose $\tilde{u}_j$ so that it is zero outside region R_{j+1} and

$$\int_{R_{j+1}} \tilde{u}_j dA = 1 \quad \text{(subarctic)}. \qquad \text{(A6)}$$

A similar interpretation of this specification can be given: the buoyancy necessary to change ρ_{j+1} into ρ_j is subtracted from the surface buoyancy flux in region R_{j+1}.

In either the subtropics or subarctic, considerable scope is still available for choosing $\tilde{u}_j(x, y)$. We chose the simplest alternative: to set $\tilde{u}_j$ equal to the inverse of the area of R_j (subtropics) or R_{j+1} (subarctic).

With these strictures, Eq. (A2) has a simple interpretation in the limiting case of continuous stratification. Integrating (A2) over a small area $dA = (Y_j - Y_{j-1})dx$ of the region R_j in the subtropics, we can show that as $Y_j \to Y_{j-1}$, $\rho_j \to \rho_{j+1}$,

$$B_0' = B_0 + \frac{g}{\rho_0}\mathbf{U}_{\mathrm{Ek}}\cdot\nabla\rho, \qquad \text{(A7)}$$

where $\mathbf{U}_{\mathrm{Ek}} = \boldsymbol{\tau}\times\hat{\mathbf{z}}/\rho_0 f$. Hence, B_0' differs from B_0 by the advection of buoyancy $-g\rho/\rho_0$ in the surface Ekman layer. Similarly, integrating (A2) over an area $dA = (Y_{j+1} - Y_j)dx$ of region R_{j+1} in the subarctic, and taking the continuous limit, we again obtain (A7) with the same interpretation.

APPENDIX B

Potential Thickness Relations and Outcrops

We consider the structure of an outcrop near the eastern boundary and how to determine it in the case of nonzero modified buoyancy flux. To make the discussion concrete consider the situation, sketched in Fig. B1, of a system of three layers labeled 2, 3, 4. The outcrop $Y_2(x)$ of layer 2 intersects the eastern boundary at y_2^e and lies along y_2^w in midocean. Along the eastern boundary the depths of the three layers are known and displayed in Fig. B1: H_4 is a constant H_{40}, and

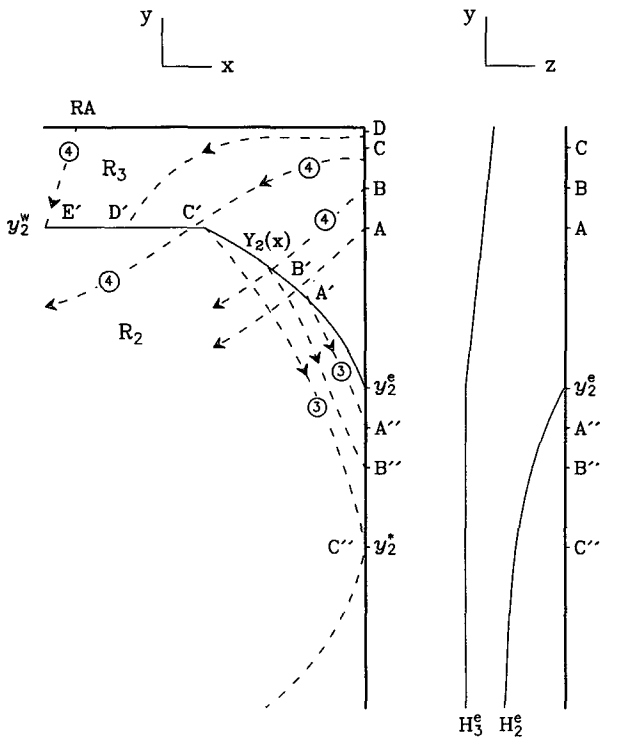

FIG. B1. Characteristics and outcrop near the eastern boundary. Outcrop is determined by shooting along characteristics of layers 3, 4 such as $AA'A''$, $BB'B''$, $CC'C''$, varying A', B', C' to match boundary conditions for layer depths at A'', B'', C'' on the eastern boundary (right panel). $CC'C''$ is the northernmost characteristic combination that can reach the eastern boundary again. Beyond C' the outcrop is chosen to be a constant latitude.

$$H_3 = H_3^e(y) = \left[H_{30}^2 + \frac{-2\tau_e^y}{\rho_0\gamma_3}(b - y)\right]^{1/2}, \quad y_2^e < y < b \qquad \text{(B.1a)}$$

$$= H_3^e(y_2^e), \quad y < y_2^e \qquad \text{(B.1b)}$$

$$H_2 = H_2^e(y) = \left[\frac{-2\tau_e^y}{\rho_0\gamma_2}(y_2^e - y)\right]^{1/2}, \quad y < y_2^e \qquad \text{(B.1c)}$$

(cf. de Szoeke 1992). At the outset suppose we know only y_2^e and must determine $Y_2(x)$ (and y_2^w), and the potential thickness relation $\Gamma_4(P_4)$. The procedure for doing this goes as follows. We already know one piece of the $\Gamma_4(P_4)$ relation: points from $y \leq y_2^e$ on the eastern boundary give the line segment $\Gamma_4 \geq (H_{40} - H_3^e(y_2^e))/f_2^e$, $P_4 = \gamma_4 H_{40}$. Start a characteristic from a point A north of y_2^e (Fig. B1); that is, integrate Eqs. (2.27), (2.28) with $k = 3$, $n = 4$, and initial conditions $x_4(t_0) = a$, $y_4(t_0) = y_A$, $H_3(t_0) = H_3^e(y_A)$, along the characteristic of layer 4, as shown. Stop the integration at some guess A' of the outcrop position of layer 2. Since the layer depths H_3, H_4 are known from the integration to this point, they can be used to compute a provisional point $P_4^{A'}$, $\Gamma_4^{A'}$ of the potential thickness relation, labeled A' on Fig. B2. Restart the integration of (2.27), (2.28) from this point with $k = 2$, $n = 4$, that is, for a characteristic of layer 3, with $H_2(t'_A) = 0$, where t'_A is the time at which an observer starts from A'. Proceed until the eastern boundary is again recrossed at A'' (Fig. B1). At this point H_4, H_3, H_2 will have reached certain values that ought to be compared with H_{40}, $H_3^e(y''_A)$, $H_2^e(y''_A)$. If they match within an acceptable tolerance, then the coordinates of A' may be accepted as a good approximation of the outcrop position and the point corresponding to A' on Fig. B2 as a good approximation of the potential thickness relation. If they do not match acceptably, the degree of mismatch may be used to devise an improved guess of the outcrop position A'. This shooting procedure may be repeated until an acceptable approximation of A' is obtained. Our experience shows that this works quite well and efficiently. Next, we may try a layer-4 characteristic starting from B, north of A, going to a guessed layer-2 outcrop position at B', returning to the eastern boundary at B'' along layer-3 characteristic, iterating until point B' is found that gives an acceptable match of depths at B''. Our experience indicates that extrapolation of points A', B', etc., produces quite good first guesses of further outcrop positions.

De Szoeke (1992) drew attention to the importance of the point y_2^* on the eastern boundary, at which $U_4 + c_{3|4} = 0$, so that a characteristic reaching this point is tangential to the boundary. The point y_2^* may be determined beforehand from (2.22), (2.24). (Note that $c_{3|4} = c_{3|3}H_3/H_4$ along the eastern boundary where $dP_4/d\Gamma_4 = 0$.) We have shown in Fig. B1 a layer-3 characteristic starting at C, going to the outcrop at C' where it joins the limiting layer-4 characteristic, which reaches the point $C''(a, y_2^*)$ (with the appropriate layer depths). The point C may be determined as accurately as desired by the above procedure. For no layer-4 characteristic sent out from any point north of C is there a choice of outcrop position that will allow it to join a layer-3 characteristic that regains the eastern boundary. Rather, the choice of outcrop beyond C' appears to be quite arbitrary. We will follow de Szoeke (1992) in

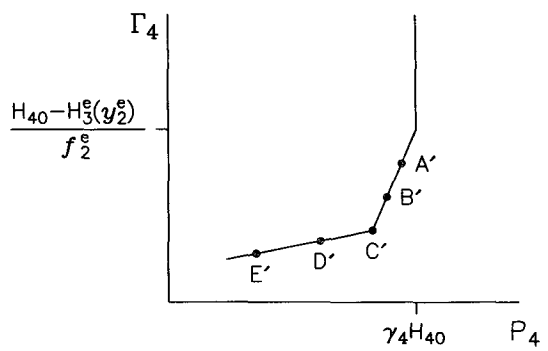

FIG. B2. Potential thickness versus pressure relation determined at the points A', B', C', D', E' in Fig. B1.

choosing the outcrop extension to be the latitude line y_2^w passing through C'. In this way, we will have determined the series of points $A', B', \ldots C'$ on Fig. B1, starting at (a, y_2^e), which define the outcrop $Y_2(x)$, and a corresponding series of points on Fig. B2 that define $\Gamma_4(P_4)$. The region bounded by the limiting characteristic $C'C''$ and its southward extension, the outcrop $Y_2(x)$, and the eastern boundary forms the analog of the region termed the eastern shadow zone for layer 3 by de Szoeke (1992). Because of buoyancy forcing, motion in this layer is not stagnant, nor is its potential thickness conserved. The eastern boundary conditions determine the segment $A'B'C'$ of the potential thickness relation $\Gamma_4(P_4)$. Hence, we call this segment the eastern boundary-ventilated portion of $\Gamma_4(P_4)$.

The latitude of the point C' defines y_2^w, which can be thought of as a function of y_2^e. The functional relation can be inverted: y_2^e can be varied, and the above procedure followed to determine outcrop and potential thickness relation until a desired y_2^w is attained. West of C' layer-4 characteristics terminating at y_2^w, such as DD' in Fig. B1, define the $\Gamma_4(P_4)$ relation along the segment $C'D' \ldots$. We call this segment of $\Gamma_4(P_4)$ the outcrop-ventilated portion.

The vertical Ekman velocity (2.7a) is chosen so that it is zero along the latitude line $y = b$: this ensures that $V_4 = 0$ [Eq. (2.23)]. Also $U_4 > 0$ along $y = b$, though decreasing eastward, while $c_{4|4} < 0$ [Eq. (2.29)]. Hence, there will be a point at which $U_4 + c_{4|4} = 0$, the location of the so-called Rossby attractor. The line $y = b$ is a layer-4 characteristic: it joins another characteristic at the attractor which strikes the layer-2 outcrop at E'. For layer 4 only, that is, the layer which is not exposed to the surface in the subtropics, we choose the $\Gamma_4(P_4)$ relation west of E' to be the extrapolation of $D'E'$ in Fig. B2. This means that H_3, H_4 are specified by the Sverdrup relation (2.9) and this relation along y_2^w west of E'. To determine H_3, H_4 in the remainder of R_3, Eqs. (2.27), (2.28) are integrated backward (in the negative t direction) starting from points along y_2^w. We do this rather than requiring homogeneous potential thickness in layer 4 along the western boundary (as we will for lighter layers) so that in the limit of zero-buoyancy forcing, layer 4 will be stagnant, as it is for LPS and de Szoeke (1992).

Outcrops of lighter layers and their potential thickness relations may be obtained in a similar way. For example, the outcrop of layer 1, given by $Y_1(x)$ and joining y_1^e and y_1^w, is found as follows. First, send out a layer-3 characteristic from the eastern boundary from a point such as A between y_1^e and y_2^* (Fig. B3), to terminate at a guessed outcrop position A'. Then restart a layer-2 characteristic at A' to return to the eastern boundary at A''. Compare the outcomes of the depths H_4, H_3, H_2, H_1 [(2.27), (2.28)] at A'' to H_{40}, $H_3^e(y_2^e)$, $H_2^e(y_1^e)$, $H_1^e(y_A'')$ and improve the guess A' until the match of depths is acceptable. This shooting

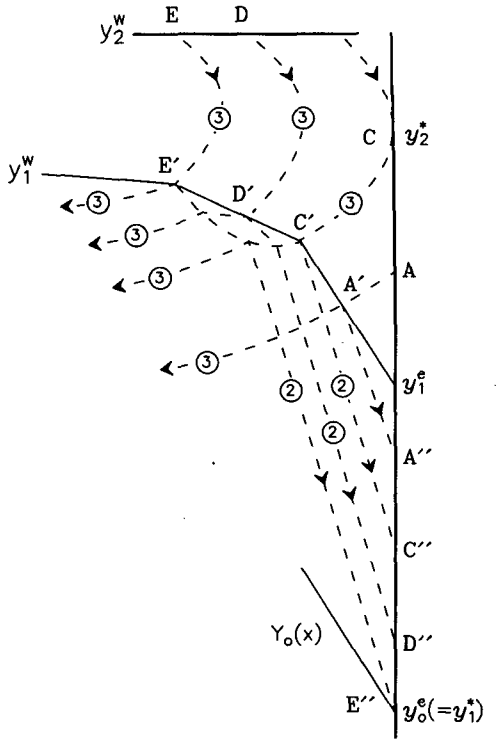

FIG. B3. Similar to Fig. B1 but for a more southerly outcrop. Characteristic combinations can begin from the eastern boundary ($AA'A''$, $CC'C''$) or from the more northerly outcrop ($DD'D''$, $EE'E''$). Beyond E' (which connects to the eastern boundary at the next outcrop E'') the outcrop is chosen to be a constant latitude.

procedure is repeated with more northerly choices of initial point A to construct the outcrop and the potential thickness relation $\Gamma_3(P_3)$. The most northerly choice of initial point on the eastern boundary is C at the latitude y_2^*: this gives the line $CC'C''$. Beyond this point layer-3 characteristics may be started from points $D, \ldots, E$ along the outcrop y_2^w. The last of these terminates on the layer-1 outcrop at E', where it joins onto a layer-2 characteristic that strikes the eastern boundary at y_1^*, which, for the same reasons as given by de Szoeke (1992), is usually taken to coincide with the position of the next outcrop (layer 0 in Fig. B3) at the eastern boundary, y_0^e. West of E' we take the layer-1 outcrop to lie along the latitude y_1^w, which E' defines. The layer depths along the outcrop $A'C'D'E'$ define $\Gamma_3(P_3)$, the potential thickness relation for the eastern shadow zone portion coming from points on the outcrop west of E'.

These remarks can be extended to cover any number of outcrops and potential thickness relations.

REFERENCES

Bennett, A. F., 1978: Poleward heat fluxes in Southern Hemisphere oceans. *J. Phys. Oceanogr.*, **8**, 785–798.

Bryan, F., 1987: Parameter sensitivity of primitive equation ocean general circulation models. *J. Phys. Oceanogr.*, **17**, 970–985.

Bryan, K., 1962: Measurements of meridional heat transport by ocean currents. *J. Geophys. Res.*, **67,** 3403–3414.

Bryden, H. L., and M. M. Hall, 1980: Heat transport by currents across 25°N latitude in the Atlantic Ocean. *Science,* **207,** 884–886.

——, D. H. Roemmich, and J. A. Church, 1991: Ocean heat transport across 24°N in the Pacific. *Deep-Sea Res.*, **38,** 297–324.

Carissimo, B. C., A. H. Oort, and T. H. Vonder Haar, 1985: Estimating the meridional energy transports in the atmosphere and ocean. *J. Phys. Oceanogr.*, **15,** 82–91.

Cox, M. D., 1984: A primitive equation, 3-dimensional model of the ocean. Tech. Rep. 1, Ocean Group, Geophysical Fluid Dynamics Laboratory, Princeton, NJ, 141 pp.

de Szoeke, R. A., 1980: On the effects of horizontal variability of wind stress on the dynamics of the ocean mixed layer. *J. Phys. Oceanogr.*, **10,** 1439–1454.

——, 1987: On the wind-driven circulation of the South Pacific Ocean. *J. Phys. Oceanogr.*, **17,** 613–630.

——, 1992: Effects of alongshore wind stress at the eastern boundary on circulation in the ocean pycnocline. *J. Phys. Oceanogr.*, **22,** 247–267.

——, and A. F. Bennett, 1993: Microstructure fluxes across density surfaces. *J. Phys. Oceanogr.*, **23,** 2254–2264.

Esbensen, S. K., and Y. Kushnir, 1981: The heat budget of the global ocean: An atlas based on estimates from surface marine observations. Oregon St. University Climatic Res. Inst. Rep. No. 29, 27 pp, 184 figs.

Gent, P. R., and J. C. McWilliams, 1990: Isopycnal mixing in ocean circulation models. *J. Phys. Oceanogr.*, **20,** 150–155.

Gill, A. E., 1982: *Atmosphere-Ocean Dynamics.* Academic Press, 662 pp.

Gregg, M. C., 1987: Diapycnal mixing in the thermocline: A review. *J. Geophys. Res.*, **92,** 5249–5286.

Haney, R. L., 1971: Surface thermal boundary condition for ocean circulation models. *J. Phys. Oceanogr.*, **1,** 241–248.

Huang, R. X., 1988: On boundary value problems of the ideal-fluid thermocline. *J. Phys. Oceanogr.*, **18,** 619–641.

Isemer, H.-J., and L. Hasse, 1987: *The Bunker Climate Atlas of the North Atlantic Ocean.* Vol. 2: *Air–Sea Interactions.* Springer-Verlag, 252 pp.

Ledwell, J. R., A. J. Watson, and C. S. Law, 1993: Evidence for slow mixing across the pycnocline from an open-ocean tracer-release experiment. *Nature,* **364,** 701–703.

Luyten, J. R., and H. Stommel, 1986: Gyres driven by combined wind and buoyancy flux. *J. Phys. Oceanogr.*, **16,** 1551–1560.

——, J. Pedlosky, and H. Stommel, 1983: The ventilated thermocline. *J. Phys. Oceanogr.*, **13,** 293–309.

McDougall, T. J., and J. A. Church, 1986: Pitfalls with the numerical representation of isopycnal and diapycnal mixing. *J. Phys. Oceanogr.*, **16,** 196–199.

Nurser, G., and J. C. Marshall, 1991: On the relationship between subduction rates and diabatic forcing of the mixed layer. *J. Phys. Oceanogr.*, **21,** 1793–1802.

Redi, M. H., 1982: Oceanic isopycnal mixing by coordinate rotation. *J. Phys. Oceanogr.*, **12,** 1154–1158.

Sellers, W. D., 1965: *Physical Climatology.* University of Chicago Press, 272 pp.

Speer, K., and E. Tziperman, 1992: Rates of water mass formation in the North Atlantic Ocean. *J. Phys. Oceanogr.*, **22,** 93–104.

Talley, L. D., 1985: Ventilation of the subtropical North Pacific: The shallow salinity minimum. *J. Phys. Oceanogr.*, **15,** 633–649.

Toole, J. M., and B. A. Warren, 1993: A hydrographic section across the subtropical South Indian Ocean. *Deep-Sea Res.*, **40,** 1973–2019.

Veronis, G., 1975: The role of models in tracer studies. *Numerical Models of Ocean Circulation.* Natl. Acad. Sci., **133–146.**

——, 1978: Model of world ocean circulation: III. Thermally and wind driven. *J. Mar. Res.*, **36,** 1–44.

Winkel, D. P., M. C. Gregg, and T. B. Sanford, 1992: Simultaneous observations of shear and turbulence in the Florida Current. *10th Symp. on Turbulence and Diffusion,* Amer. Meteor. Soc., 101–104.

Yin, F. L., I. Y. Fung, and C. K. Chu, 1992: Equilibrium response of ocean deep-water circulation to variations in Ekman pumping and deep-water sources. *J. Phys. Oceanogr.*, **22,** 1129–1157.